



# Light absorption properties of mesoporous barium hexaferrite, BaFe<sub>12</sub>O<sub>19</sub>

Alan Bañuelos-Frías<sup>a</sup>, Gerardo Martínez-Guajardo<sup>b</sup>, Leo Alvarado-Perea<sup>a,b</sup>, Lázaro Canizalez-Dávalos<sup>b</sup>, Facundo Ruiz<sup>c</sup>, Claudia Valero-Luna<sup>a,\*</sup>

<sup>a</sup> Unidad Académica de Ingeniería Eléctrica, Universidad Autónoma de Zacatecas, Zac 98000, Mexico

<sup>b</sup> Unidad Académica de Ciencias Químicas, Universidad Autónoma de Zacatecas, Zac 98160, Mexico

<sup>c</sup> Facultad de Ciencias, Universidad Autónoma de San Luis Potosí, S.L.P 78290, Mexico

## ARTICLE INFO

### Article history:

Received 16 March 2019

Received in revised form 18 May 2019

Accepted 29 May 2019

Available online 30 May 2019

### Keywords:

Bandgap

Barium hexaferrite

Kubelka-Munk method

## ABSTRACT

Light absorption properties are one of the most important characteristics of semiconductor materials, since it is related to particle size, electric resistance, powder density, and dielectric constant. Barium hexaferrite (BaFe<sub>12</sub>O<sub>19</sub>) particles were synthesized by ceramic and chemical co-precipitation method. Light absorption properties were studied in relation to the particle size, morphology, and surface porosity. The band gap was calculated by the Kubelka-Munk method from the obtained experimental absorption spectrum. Band gap energies of 1.82 and 1.86 eV were estimated for the particles synthesized by the ceramic method and for the co-precipitation method respectively. The results show that both synthesized BaFe<sub>12</sub>O<sub>19</sub> samples can be effectively excited with visible light irradiation. In addition to this, due to its other good characteristics such as its magnetic properties, high resistance to corrosion, and chemical stability, make the barium hexaferrite an excellent material for diverse technological applications.

© 2019 Elsevier B.V. All rights reserved.

## 1. Introduction

There are diverse methodologies for the estimation of the band gap energy for semiconductor materials, from optical to electrochemical [1–5]. The most common method used is the diffuse reflectance method, in which the absorption spectrum of the studied material is analyzed [1,2,6]. Semiconductors are mainly used as catalysts, solar cells, lasers, Gamma ray detectors, and electronic devices due to their efficient charge transference and their photon absorption properties [7,8]. Materials as MFe<sub>2</sub>O<sub>4</sub>, (where, M = Ba, Zn, Fe, Co, Cu, Mn), BiFeO<sub>3</sub>, BaFe<sub>3-x</sub>, present a band gap energy of ~2 eV, therefore, are efficiently excited under visible light irradiation [9–16] and in addition, has excellent magnetic properties [16–22]. MFe<sub>12</sub>O<sub>19</sub> (where, M = Ba, Sr, Cu, Pb) [19,23–25] magnetic properties are known to be highly dependent of the electronic configuration of the substituting cations as well as on their site preference into the structure [26–29]. Barium hexaferrite is a semiconductor material, technologically important due to its low production cost and by its multiple applications as permanent magnets, as high density recording devices, speaker components,

electric motors, microwave devices, and recently as catalysts [10,11,15,16,30–32]. In addition, Barium hexaferrite possesses exceptional properties as high Curie temperature, high cohesive strength, high magnetic field anisotropy, chemical stability, and corrosive resistance [30,32,33]. The goal of this work is to synthesize the BaFe<sub>12</sub>O<sub>19</sub> by both ceramic and chemical co-precipitation method, and then study and to compare their band gap energy as a part of their optical properties, according to the particle size, morphology, surface area, and porosity.

## 2. Materials and methods

For the synthesis of the BaFe<sub>12</sub>O<sub>19</sub> by the ceramic method, a mixture of barium carbonate and iron oxide was used, then the mixture was sintered at 1473 K, as reported by Ataie et al [34]. On the other hand, for the synthesis by the chemical co-precipitation method, barium nitrate and iron nitrate salts were precipitated at pH = 11 and then sintered at 1173 K, as reported in our previous work [15].

The BaFe<sub>12</sub>O<sub>19</sub> crystalline phase was determined by the use of an X-ray diffractometer Bruker-AXS D8 Advanced with CuK radiation ( $\lambda = 1.5406 \text{ \AA}$ ). The particle size and morphology were studied by Transmission Electron Microscopy (TEM, JEOL

\* Corresponding author.

E-mail address: [cvalero@uaz.edu.mx](mailto:cvalero@uaz.edu.mx) (C. Valero-Luna).



Contents lists available at ScienceDirect

# Superlattices and Microstructures

journal homepage: [www.elsevier.com/locate/superlattices](http://www.elsevier.com/locate/superlattices)

## TM plasmonic modes in a multilayer graphene-dielectric structure

J. Madrigal-Melchor<sup>a,\*</sup>, J.S. Pérez-Huerta<sup>a</sup>, J.R. Suárez-López<sup>a</sup>, I. Rodríguez-Vargas<sup>a</sup>,  
D. Ariza-Flores<sup>b</sup>

<sup>a</sup>Unidad Académica de Física, Universidad Autónoma de Zacatecas, Calzada Solidaridad Esquina Paseo a la Bufa s/n, CP 98060, Mexico

<sup>b</sup>CONACYT-Instituto de Investigación en Comunicación Óptica, Universidad Autónoma de San Luis Potosí, Av. Karakorum 1470, Lomas 4a sección, San Luis Potosí, SLP 78210, Mexico



### ARTICLE INFO

#### Keywords:

Graphene  
Plasmons on surfaces and interfaces  
Transversal magnetic polarization  
Attenuated total reflection  
Optical properties of multilayers

### ABSTRACT

Optical and electronic properties of multilayer systems have been extensively studied in the last years due to its potential applications in high-performance optoelectronic and photonic devices. In particular, the role of plasmonic modes is critical in such systems leading to improvements in solar cells efficiency, detection of biosensors, Raman signal enhancement, among others. In this work, we study the plasmonic modes in a multilayer system composed of graphene layers embedded within dielectric materials. The dispersion relation of plasmonic modes is obtained by calculating the poles of reflectivity using the transfer matrix method. We show the attenuated total reflection spectra for a multilayer graphene-dielectric structure, and determine the optimum distance between the prism and the multilayer system for detecting graphene plasmons in the Otto configuration. Additional to the well-known plasmonics bands, when we consider the interband and intraband contribution of graphene's conductivity, and large wavevectors parallel to graphene's plane, all plasmonic bands have an asymptotic behavior. Besides, an upper mode emerges. Finally, it is important to highlight that the number of branches in the plasmonic relation dispersion depend on the number of graphene sheets.

### 1. Introduction

Plasmonics studies the interaction between electromagnetic radiation and the conduction electrons at a metallic interface. As a branch of nanophotonics, this field has a great interest because it takes advantage of the manipulation, control, and coupling of light at subwavelength dimensions, enhancing the electromagnetic field confinement and also breaking the Abbe limit of diffraction [1–3].

Plasmons have been studied for decades; the first studies about plasmons came in late 1890 and early 1900 with the works of Sommerfeld [4], Zenneck [5] and Wood [6], who studied the interaction between light and metallic media. On the other hand, it is well known that collective excitation of free charge in metallic surfaces, i.e., surface plasmons (SP), can be coupled with the electromagnetic radiation as a surface plasmon polariton (SPP), and play a key role in a broad spectrum of science, ranging from physics and material science to biology and medicine [2,7,8], and references therein. The term plasmon was coined by Ritchie in 1957 [9] and since then it has been extensively studied due to its optical and electrical properties which allow to have diverse applications as waveguides sources, near-field optics, data storage devices, solar cells, surface-enhancement Raman spectroscopy (SERS), chemical sensors and biosensors, see Ref. [2] and references therein. Moreover, it is well known that a multilayer structure of metallic films

\* Corresponding author.

E-mail address: [jmadrigal.melchor@fisica.uaz.edu.mx](mailto:jmadrigal.melchor@fisica.uaz.edu.mx) (J. Madrigal-Melchor).

URL: <http://fisica.uaz.edu.mx/jmadrigal.melchor> (J. Madrigal-Melchor).

<https://doi.org/10.1016/j.spmi.2018.11.015>

Received 15 September 2018; Received in revised form 8 November 2018; Accepted 19 November 2018

Available online 23 November 2018

0749-6036/ © 2018 Elsevier Ltd. All rights reserved.



# Tailoring the transmission and absorption spectra in a graphene-dielectric multilayer system for Lorentzian profile in the chemical potential



A. Sánchez-Arellano<sup>a</sup>, J.S. Pérez-Huerta<sup>a</sup>, D. Ariza-Flores<sup>b</sup>, I.A. Sustaita-Torres<sup>c</sup>,  
J. Madrigal-Melchor<sup>a,\*</sup>

<sup>a</sup>Unidad Académica de Física, Universidad Autónoma de Zacatecas, Calzada Solidaridad esquina Paseo a la Bufa s/n, CP 98060, Mexico

<sup>b</sup>CONACYT-Instituto de Investigación en Comunicación Óptica, Universidad Autónoma de San Luis Potosí, Av. Karakorum 1470, Lomas 4a sección, San Luis Potosí, SLP 78210, Mexico

<sup>c</sup>Unidad Académica de Ingeniería Eléctrica, Universidad Autónoma de Zacatecas, Av. Ramón López Velarde 801, CP 98000, Mexico

## ARTICLE INFO

### Keywords:

Graphene  
Graphene transmission  
Graphene absorption  
Optical properties of multilayers

## ABSTRACT

In this work, we show how to modulate the transmission, reflection, and absorption spectra of a dielectric-graphene multilayer structure, by tailoring the profile on the chemical potential of the graphene sheets, through a discrete Lorentzian profile for the chemical potential ( $\mu_g$ ) as a function of the depth of the proposed structure. Whereas the reflection spectrum is slightly affected with the stack of graphenes, but transmission and absorption spectra are modulated in a frequency region where there is no absorption as compared to a single or multilayer system with constant  $\mu_g$ . Additionally, we develop and test an analytic expression that predicts the asymptotic behavior for transmission and absorption for different numbers of graphene sheets, dielectric host media, incident angle, and light polarization. Finally, we explain the physical differences between the spectra obtained for TM and TE polarizations of the incident light on the structure.

## 1. Introduction

Electromagnetic waves propagation in periodic [1,2] and aperiodic [3–5] structures has been an essential subject of research since the last century, due to the ability of such systems to modulate the flow of light. For instance, these structures can be designed to have a wide stop-band (or pass-band) range of frequencies where the electromagnetic waves cannot be propagated (or can be fully propagated), which is suitable for the applications in optical filters [6], waveguides, among others [7,8]. Another type of multilayer structures are the dielectric-metal stacks. In this case, the absorption of the metallic layers plays an important role in the photonic structure, and the optical response is strongly modified in comparison with a nonabsorbent superlattice [9,10]. Similarly, multilayered systems where the constituent layers follow a profile modulated with different physical parameters that characterize the material have been studied by several groups [11–16]. For example, Tung et al., reported the electronic properties of a multilayer semiconductor system for a Gaussian profile in the concentration of carriers [11]. Through this modification, they showed that the desired pass-band or stop-band of the structure can be obtained. Yamada et al., showed a method based on the inverse Fourier transform of the refractive index in order to design an optical filter [12]. Moreover, our research group has shown the possibility to

\* Corresponding author..

E-mail address: [jmadrim@uaz.edu.mx](mailto:jmadrim@uaz.edu.mx) (J. Madrigal-Melchor).

URL: <https://jesusmadrigalmelchor.wordpress.com/> (J. Madrigal-Melchor).

<https://doi.org/10.1016/j.spmi.2019.04.014>

Received 19 January 2019; Received in revised form 1 April 2019; Accepted 11 April 2019

Available online 16 April 2019

0749-6036/ © 2019 Elsevier Ltd. All rights reserved.

## Synthesis and Characterization of Hydrogels with Ag Nanoparticles

K. G. H Martínez-Reyna; M. G. García-Valdivieso; H. R. Navarro-Contreras

Laboratorio Nacional CIACYT-Universidad Autónoma de San Luis Potosí, Av. Sierra Leona 550, Col. Lomas 2a. Sección, C.P 78210, San Luis Potosí, S.L.P., MÉXICO.

### ABSTRACT

*Hydrogels made of sodium 2-acrylamide-2-methylpropanesulfonate were synthesized with the goal of creating a polymer for tissue engineering applications. The hydrogels were doped with silver nanoparticles to create hydrogel/Ag with possible antibacterial properties. We varied the weight/volume percentage of Laponite from 3 to 10 w/v% to alter the rheological properties of the hydrogels. Raman spectroscopy was used to study the progress of the chemical reaction at different polymerization times under ultraviolet radiation. By comparing the changes in the intensities of the Raman bands corresponding to C=C and C–C bonds with reaction time, we found that the optimal polymerization time to obtain chains of poly(2-acrylamide-2-methylpropanesulfonate) was 3 to 4 h. Characterization of the hydrogels with scanning electron microscopy indicated pore sizes of 1 to 6  $\mu\text{m}$ .*

### INTRODUCTION

Hydrogels are of great interest because of their unique properties, including ability to absorb large volumes of water, softness, flexibility and biocompatibility [1]. Hydrogels are three-dimensional, hydrophilic, polymeric networks capable of absorbing large amounts of water or biological fluids. Based on these properties, hydrogels have numerous applications in drug delivery, pesticides and tissue engineering. Tissue engineering is a method used to regenerate damaged tissue or replace organs in the body [2]. For example, injuries to menisci are the second most common knee injury, with an incidence of 61 cases per 100,000 persons [3]. This injury is common in young people (under 40 years) and especially athletes, along with patients over 65 years of age [4]. Currently, meniscus injuries are treated using transplants. While Verdonk et al. reported that 75%–90% of patients experienced fair to excellent functional results after meniscal



# Nitrogen doped carbon nanotubes decorated with iron carbide nanoparticles and their electrochemical capacitance



E. Tovar-Martinez<sup>a</sup>, J.V. Cabrera-Salazar<sup>a</sup>, D. Hernandez-Arriaga<sup>b</sup>, M. Reyes-Reyes<sup>b,\*</sup>, Luis F. Chazaro-Ruiz<sup>c</sup>, R. López-Sandoval<sup>a,\*</sup>

<sup>a</sup> Advanced Materials Department, IPICYT, Camino a la Presa San José 2055, Col. Lomas 4a sección, San Luis Potosí 78216, Mexico

<sup>b</sup> Instituto de Investigación en Comunicación Óptica, Universidad Autónoma de San Luis Potosí, Álvaro Obregón 64, San Luis Potosí 78000, Mexico

<sup>c</sup> Environmental Science Department, IPICYT, Camino a la Presa San José 2055, Col. Lomas 4a sección, San Luis Potosí 78216, Mexico

## ARTICLE INFO

### Keywords:

Carbon nanotubes  
Electrochemical capacitors

## ABSTRACT

Different ethanol-benzylamine (EB) ratio (9/1 v/v and 1/1 v/v) reaction mixtures were prepared for the synthesis of nitrogen doped multiwalled carbon nanotubes (N-MWCNTs). The morphology of the synthesized sample depends of the used catalyst percentage, 1 wt% or 3 wt%, during the synthesis. In low ferrocene concentration, EB91-1 wt % and EB11-1 wt% samples are mainly composed by N-MWCNTs with iron-carbide nanoparticles at their tips, whereas at high ferrocene concentration, EB91-3 wt % and EB11-3 wt% samples are composed by a mix of N-MWCNTs and carbon nano-onions (CNOs) with iron-carbide core. The way in which CNOs are distributed in EB91-3 wt% and EB11-3 wt% samples is related to the ethanol ratio used in the reaction mixture. In EB91-3 wt% sample, CNOs are distributed more homogeneously on the surfaces of the N-MWCNTs, while EB11-3 wt% sample, CNOs are segregated from N-MWCNTs. High ethanol ratio in the reaction mixture increases the probability of attaching oxygenated groups on N-MWCNTs surfaces, i.e. the surfaces functionalization is carried out during the synthesis, making possible CNOs anchoring on N-MWCNTs walls. This difference in morphology in the sample plays an important role for the high electrochemical capacitance in the EB91-3 wt% samples compared with other samples.

## 1. Introduction

Carbon nanotubes (CNTs) are carbon allotropes, which arise from rolling a graphene sheet in a tubular form. In 1991, Iijima reported the first multi-walled carbon nanotubes (MWCNTs) obtained from soot using the arc discharge method [1]. Two years later, he reported the existence of single-walled carbon nanotubes (SWCNTs) [2]. There are several methods to synthesize CNTs, being the most populars laser ablation, electrolysis, arc discharge and chemical vapor deposition. Each of these methods has its advantages and disadvantages, which are related with different CNTs growth mechanisms, and this in turn, generate CNTs with different particular properties. Due to the possible applications of energy storage devices, such as in portable electronics, in power supply devices and in electric vehicles, supercapacitors based on carbon nanostructures have attracted significant interest for their research [3,4]. The operation of these devices is due to the formation of electric double layers (EDL), which gives a high electrochemical performance, as well as high power density, long life cycles and relatively low costs [5–7]. In contrast to activated carbon (ACs) [8], MWCNTs

have a relatively low specific surface area (SSA) and, consequently, a low density of energy storage [8,9]. However, while the low SSA of MWCNTs limits their capacitance, their high electrical conductivity and open porosity allow a rapid ions transport and, in this way, they show good electrical power characteristics [8]. In general, for their use as EDLCs, MWCNTs are treated in acids to increase their SSA, thus their capacitance, as well as their processability [10–13]. Depending on the type of MWCNTs and the acid treatment, capacitances in the range of 4–80 F g<sup>-1</sup> have been reported [13]. Moreover, it has been shown that the treatment of MWCNTs in concentrated nitric acid (69%) at 80 °C for 1 h increases the amount of oxygenated groups on the surface as well as its SSA to 475 m<sup>2</sup> g<sup>-1</sup>, giving rise to an increase in the capacitance of 137 F g<sup>-1</sup> [13]. However, the oxygenated groups on the surface of the MWCNTs, which were responsible for the high capacitance, caused self discharge in the capacitor, thus, these highly oxidized MWCNTs will have a very limited application [13]. On the other hand, it has been fabricated nanocomposite electrodes using different kinds of carbon nanostructures and MWCNTs. In the case of Carbon-MWCNTs (C-MWCNTs) nanocomposite electrodes, after nitric acid treatment of

\* Corresponding authors.

E-mail addresses: [reyesm@iico.uaslp.mx](mailto:reyesm@iico.uaslp.mx) (M. Reyes-Reyes), [sandov@ipicyt.edu.mx](mailto:sandov@ipicyt.edu.mx) (R. López-Sandoval).

<https://doi.org/10.1016/j.mtcomm.2019.100667>

Received 19 June 2019; Received in revised form 6 September 2019; Accepted 26 September 2019

Available online 27 September 2019

2352-4928/ © 2019 Elsevier Ltd. All rights reserved.



# Effect of temperature on the magnetic properties of strontium hexaferrite synthesized by the Pechini method

M. A. Urbano-Peña<sup>1</sup> · S. A. Palomares-Sánchez<sup>1</sup> · I. Betancourt<sup>2</sup> · T. J. Pérez-Juache<sup>3</sup> · F. Ruiz<sup>1</sup>

Received: 1 August 2019 / Accepted: 10 September 2019 / Published online: 19 September 2019  
© Springer-Verlag GmbH Germany, part of Springer Nature 2019

## Abstract

In this work, strontium hexaferrite powders were synthesized by the polymeric complex method (Pechini). The as-prepared samples were calcined at temperatures of 800 °C, 850 °C, 900 °C, 1000 °C, and 1050 °C for 1 h. In addition, the presence of a secondary phase of hematite ( $\alpha$ -Fe<sub>2</sub>O<sub>3</sub>) was detected in all samples. The influence of calcination temperature and synthesis technique to control grain growth and size was analyzed. The crystalline phases, structure and morphology of the samples were determined by X-ray diffraction, scanning electron microscope and transmission electron microscopy. While the magnetic properties were measured at room temperature using a vibrating sample magnetometer with an applied field of up to 20 KOe. The results show that the sample calcined at 900 °C with a crystal size of 245 nm exhibits the best magnetic properties of the entire series, obtaining the highest values of magnetization by saturation and coercivity ( $M_s$  99.3 emu/g, and  $H_c$  6.15 kOe). This can be attributed to the exchange coupling interactions between the soft and hard phases of the sample.

## 1 Introduction

The M-type hexaferrites are ferrites with hexagonal structure with general formula  $MFe_{12}O_{19}$  ( $M = Ba, Sr, Pb, Ca, La$ ), and belong to the class of ferromagnetic oxides. Since their discovery in 1950, hexaferrites have been widely used as permanent magnets [1]. Currently, the most used magnetically hard materials in the industry as permanent magnets are M-type hexaferrite due to their low production costs, high corrosion resistance, low electrical conductivity, chemical stability and high magnetic anisotropy [2]. Among its applications, we can highlight its use in electronic devices [3], electric motors [4], thermoelectric power generation [5], gas sensors, catalyst for the degradation of some pollutants [6, 7], telecommunications [8], and, recently, in biomedical applications such as drug delivery systems, hyperthermia

in cancer therapy [9, 10], and contrast agents for magnetic resonance [11].

To modify the magnetic properties of M-type hexaferrite, research has focused on the substitution with one or more elements in the Fe<sup>3+</sup> and/or Sr<sup>2+</sup> ion sites such as Al, Cu, Co, Mn, Ti, Zn, and Zr [12–15], due to the reported increase in coercivity.

Additionally, partial substitutions of Fe<sup>3+</sup> and/or Sr<sup>2+</sup> ions sites by elements of the rare earth family such as Ce [16], Tm [17], Pr [13], Nd [18, 19], Th [20], La [21], Er [22], Sm [15, 23] and Ga [24]. However, due to the limited availability of elements belonging to the rare earths group, their use in the production of M-type hexaferrites significantly increases the costs of the material, resulting in a low rentability of the product for industrial use.

Also, it should be noted that the magnetic properties such as extrinsic parameters (coercivity, remnant magnetization, shape and particle size) and intrinsic parameters (saturation magnetization, magnetocrystalline anisotropy, anisotropy constant, Curie temperature) of hexaferrites depend on their chemical composition, structure, sintering temperature, etc. These parameters can be controlled by the substitution of ions in their formula, as mentioned above, but also by the variation of pH, temperature, grain size, reaction speed and heat treatment time, through different synthesis methods such as sol–gel [25], polymer complex (Pechini) [26], solid-state [27], co-precipitation [28], glass crystallization

✉ M. A. Urbano-Peña  
mariangeles137@hotmail.com

<sup>1</sup> Facultad de Ciencias, Universidad Autónoma de San Luis Potosí, Av. Parque Chapultepec 1570, 78210 San Luis Potosí, Mexico

<sup>2</sup> Dpto. Materiales Metálicos y Cerámicos, Instituto de Investigaciones en Materiales, Universidad Nacional Autónoma de México, CDMX 04510, Mexico

<sup>3</sup> Escuela Nacional de Estudios Superiores, Universidad Nacional Autónoma de México, Morelia, Mexico

## When is a dynamical system mean sensitive?

FELIPE GARCÍA-RAMOS†‡, JIE LI§¶ and RUIFENG ZHANG||

† *Instituto de Física, Universidad Autónoma de San Luis Potosí, Manuel Nava 6,  
SLP, Mexico 78290*

*(e-mail: felipegra@yahoo.com)*

‡ *Catedras CONACyT, Av. Insurgentes Sur 1582, Del. Benito Juárez, Mexico City,  
Mexico 03940*

§ *School of Mathematics and Statistics, Jiangsu Normal University, Xuzhou,  
Jiangsu, 221116, PR China*

*(e-mail: jiel0516@mail.ustc.edu.cn)*

¶ *Academy of Mathematics and Systems Science, Chinese Academy of Sciences, Beijing,  
100190, PR China*

|| *School of Mathematics, Hefei University of Technology, Hefei, Anhui, 230009,  
PR China*

*(e-mail: rfzhang@mail.ustc.edu.cn)*

*(Received 14 February 2017 and accepted in revised form 4 August 2017)*

*Abstract.* This article is devoted to studying which conditions imply that a topological dynamical system is mean sensitive and which do not. Among other things, we show that every uniquely ergodic, mixing system with positive entropy is mean sensitive. On the other hand, we provide an example of a transitive system which is cofinitely sensitive or Devaney chaotic with positive entropy but fails to be mean sensitive. As applications of our theory and examples, we negatively answer an open question regarding equicontinuity/sensitivity dichotomies raised by Tu, we introduce and present results of locally mean equicontinuous systems and we show that mean sensitivity of the induced hyperspace does not imply that of the phase space.

### *Contents*

1	Introduction	1609
2	Preliminaries	1612
3	Main results	1616
4	Applications	1629
	Acknowledgements	1635
	References	1635



## Spray-on thermoelectric energy harvester

Robert E. Peale,<sup>1,2</sup> Seth Calhoun,<sup>1</sup> Nagendra Dhakal,<sup>1</sup> and Isaiah O. Oladeji<sup>1,3</sup> Francisco J. González<sup>1,4</sup>

<sup>1</sup>Physics, University of Central Florida, Orlando FL 32816

<sup>2</sup>Truventic LLC, 1209 W. Gore St. Orlando FL 32805

<sup>3</sup>SISOM Thin Film LLC, 1209 W. Gore St. Orlando FL 32805

<sup>4</sup>Terahertz Science and Technology National Lab (LANCyTT), Universidad Autónoma de San Luis Potosí, Mexico

### ABSTRACT

*Thermoelectric (TE) thin films have promise for harvesting electrical energy from waste heat. We demonstrate TE materials and thermocouples deposited by aqueous spray deposition on glass. The n-type material was CdO doped with Mn and Sn. Two p-type materials were investigated, namely PbS with co-growth of CdS and doped with Na and Na<sub>2</sub>CO<sub>4</sub>. Seebeck coefficients, resistivity, and power generation for thermocouples were characterized.*

### INTRODUCTION

Thin-film thermoelectric energy harvesters have been suggested for long-flight-duration un-manned aerial vehicles [1]. Temperature gradients of ~1 deg C per cm occur along aircraft skins [2]. Waste heating of vehicle exhaust systems can give surface lateral temperature gradients exceeding 2 deg C per cm [3]. Such offer opportunity for energy harvesting using thin film thermocouples applied as paint-like coatings. This paper investigates thermoelectric thin films prepared by an aqueous spray process.



# Berry-Phase in a Periodically Driven Single Molecule Magnet Transistor

Gabriel González

The electron transport through a single molecule magnet transistor in the presence of a local transverse magnetic field and ac-driven gate voltage has been considered. The conductance has been calculated as a function of the electron energy and transverse magnetic field by using the Floquet and Landauer formalism. It is shown that the time periodic potential causes zero transmission resonances that oscillate as a function of the transverse magnetic field due to the Berry phase interference associated with two quantum tunneling paths. It has been found that these Berry phase oscillations can be detected in the conductance as a function of the transverse magnetic field for an incoming electron with a specific energy.

## 1. Introduction

Considerable efforts have been devoted to the constant miniaturization of electronic devices in the semiconductor-based industry. The idea to use single molecules as electronic components appeared for the first in the 1974,<sup>[1]</sup> but it had to wait until the appearance of nanoscience which enable individual molecules to be connected between two contact leads.<sup>[2]</sup> Recently, a number of experimental studies have been conducted to study electron transport through a single molecule magnet (SMM).<sup>[3]</sup> SMM, such as Mn<sub>12</sub> (see ref. <sup>[4]</sup>) and Fe<sub>8</sub> (see ref. <sup>[5]</sup>), have been a topic of research of growing interest in the nanoscience since experiments in bulk samples provided for the first time evidence of quantum spin tunneling at low temperatures and Berry-phase interference effects in the presence of a transverse magnetic field which leads to a vanishing of the energy splitting.<sup>[6,7]</sup> Remarkably, a transverse magnetic field can be tuned to topologically quench the two resonant spin states of a SMM.<sup>[8–12]</sup> Electron transport through a SMM in a three terminal configuration have already been studied in several experiments where they have shown the Coulomb

blockade. Oscillations of the Kondo effect as a function of the transverse magnetic field were also investigated.<sup>[13,14]</sup> Theoretical evidence of the Berry-phase interference effect in electron transport in a SMM transistor with opposite spin-polarized leads have also been studied.<sup>[15]</sup> On the theoretical side, the electron transport properties in a SMM transistor were mostly investigated within a constant gate voltage. More recently, the problem of electron transport through a periodically driven ferromagnetic quantum barrier with a local magnetic field and ac-driven potential was solved using the Floquet formalism.<sup>[16]</sup>

In this letter, we present a theoretical study of the Berry-phase effect in electron transport through a SMM transistor under a local time periodic gate voltage and a transverse magnetic field, and show that the time periodic potential causes zero transmission resonances that oscillate as a function of the transverse magnetic field due to the Berry phase interference associated with two quantum tunneling paths. We show that the Berry phase oscillations can be detected in the conductance of the SMM transistor. In particular, we study the electron transmission through a SMM connected to two contacts with a local transverse magnetic field and a oscillating gate voltage as illustrated in **Figure 1**.

## 2. Model Hamiltonian

We consider transport of unpolarized incoming electrons modeled by a one dimensional tight-binding chain with nearest neighbor hopping amplitude  $J$ . Taking the on-site energy equal to zero and  $\hbar = 1$ , the effective Hamiltonian reads

$$\mathcal{H}_{\text{leads}} = -J \sum_{i>0(i<0)} \sum_{\sigma} (c_{i,\sigma}^{\dagger} c_{i+1,\sigma} + c_{i+1,\sigma}^{\dagger} c_{i,\sigma}) \quad (1)$$


where  $c_{i,\sigma}^{\dagger}$  and  $c_{i,\sigma}$  are the creation and annihilation operators at the  $i$ th site with spin  $\sigma$ , respectively.

The simplest effective Hamiltonian which describes the Berry-phase of the spin quantum tunneling in SMMs is the so-called giant spin approximation (GSA) model,<sup>[17]</sup> and with a local periodically driven gate voltage with angular frequency  $\omega$  and amplitude  $V_g$  we can write the AC-GSA Hamiltonian as

$$\mathcal{H}_{\text{AC-GSA}} = \mathcal{H}_{\text{GSA}} + \sum_{\sigma} (\epsilon_{0L} - V_g \cos(\omega t)) c_{0,\sigma}^{\dagger} c_{0,\sigma} + U n_{0,\uparrow} n_{0,\downarrow} \quad (2)$$

Dr. G. González  
Cátedra CONCAYT  
Universidad Autónoma de San Luis Potosí  
San Luis Potosí 78000, Mexico  
E-mail: gabriel.gonzalez@uaslp.mx

Dr. G. González  
Coordinación para la Innovación y la Aplicación de la Ciencia y la Tecnología  
Universidad Autónoma de San Luis Potosí  
San Luis Potosí 78000, Mexico

 The ORCID identification number(s) for the author(s) of this article can be found under <https://doi.org/10.1002/pssb.201800725>.

DOI: 10.1002/pssb.201800725

# Taming Emerging Devices' Variation and Reliability Challenges with Architectural and System Solutions [Invited]

Yuyang Wang<sup>1</sup>, Leilai Shao<sup>1</sup>, Miguel Angel Lastras-Montañó<sup>2</sup>, Kwang-Ting Cheng<sup>3</sup>,

<sup>1</sup>*Department of Electrical and Computer Engineering, University of California, Santa Barbara, U.S.A.*

<sup>2</sup>*Instituto de Investigación en Comunicación Óptica, FC, Universidad Autónoma de San Luis Potosí, México*

<sup>3</sup>*School of Engineering, Hong Kong University of Science and Technology, Hong Kong*

**Abstract**—Emerging devices are promising alternatives to traditional CMOS technologies as proposed in various solutions for future computation and communication systems. However, such devices often suffer from significant variations and relatively poor reliability. To address such limitations for their broader adoption, novel techniques at circuit, architecture, and system levels could help alleviate the device variation and reliability challenges. In this paper, we illustrate the effectiveness of such techniques in three distinct application domains, namely non-volatile memories, flexible electronics, and silicon photonics-enabled optical interconnects.

## I. INTRODUCTION

The CMOS integrated circuits have experienced enormous success in the past few decades through continuous technology scaling, which shaped today's industrial and consumer electronics. However, with the scaling rate gradually slowing down and to eventually hit the atomistic and quantum mechanical physics boundaries [1], traditional CMOS technologies may prove inadequate to accommodate the rapid growth of future computation- and communication-hungry applications, as well as new sensing applications which require innovative forms of interfaces to humans. Alternative material and devices are being actively investigated to assist, and potentially replace, traditional silicon electronics in emerging application domains such as next-generation non-volatile memories, flexible electronics, optical interconnects, spintronics, quantum computing, etc. Despite promising results demonstrated by theoretical derivations and prototypes, emerging devices often suffer from significant process variations and reliability issues due to immature fabrication techniques. Such limitations must be tackled before any broad adoption can take place. In addition to the efforts put into device optimization and process control, innovative techniques applied at circuit, architecture, and system levels could also help alleviate the variation and reliability challenges.

NAND flash, for instance, is a non-volatile memory (NVM) technology that successfully tackled these limitations and now it is virtually everywhere, from cheap USB thumb drives to mobile devices and enterprise storage applications. Among architectural solutions, memory cell disturbs while reading and writing adjacent cells was reduced by changing the conventional half-bit-line (HBL) architecture to the all-bit-line (ABL) architecture, which reduced by half the stress on the bit lines. Low reliability margins are addressed with stronger error correcting codes, as well as with system-level algorithms to tune the memory chip for a specific type of application (e.g. read- versus write-intensive applications). The premature death

of memory blocks due to the limited endurance of the memory cells (i.e. the maximum number of times a cell can be reliably written into) is prevented with wear-leveling algorithms, that aim to distribute memory writes as evenly as possible. An undesired effect of this is that the same logical data may be present in more than one physical location in the memory, a phenomenon known as write amplification. This last problem is typically overcome by over-provisioning the memory, i.e., by providing extra physical storage capacity that is not visible to the user.

In the rest of this paper, we use three specific examples, namely non-volatile memories, flexible electronics, and silicon photonics-enabled optical interconnects, to illustrate the recent progress of circuit-, architecture-, and system-level techniques applied to emerging devices and their effectiveness in variation and reliability management.

## II. NON-VOLATILE MEMORIES

### A. Introduction

The need for larger, faster, and lower-power memories has been addressed so far by aggressive technology downscaling and operating voltage reduction. Dynamic random-access memory (DRAM) and NAND flash, as the current prominent technologies for main memory and storage, respectively, have been following this trend. However, the ever-increasing performance gap between them has rendered a memory system solely based on these two technologies inadequate in the long term [2]. Resistive random-access memory (ReRAM) based on two-terminal resistance switching memristive devices is a promising contender to fill such gap. ReRAM, a non-volatile memory (NVM) technology, offers memory densities that are comparable to those of NAND flash, and fast random accesses that are comparable to those of DRAM, effectively offering the advantages of both technologies [3].

### B. Memristive Devices and ReRAM Architectures

The main memory element in a ReRAM unit cell is the memristor, whose characteristic feature is the so-called pinched hysteresis loop in its current-voltage (I-V) plane [4], as shown in Fig. 1(a). Due to its structural simplicity (two electrodes sandwiching a thin oxide layer, as shown in Fig. 1(b)), an array of memristors can be organized in a crossbar fashion, in which at each cross-point, a memristor is formed (Fig. 1(c)). This is known as the 1TnR architecture, and it is the preferred ReRAM architecture from the density point of view, as every electrode is connected to  $n$  memristors and one transistor is

## Electrostatic simulation of the Jackiw-Rebbi zero energy state

G. González<sup>a,b</sup>, J. Méndez-Lozoya<sup>b</sup>, R. Díaz de León-Zapata<sup>b,c</sup> and F. Javier González<sup>b</sup>

<sup>a</sup>*Cátedras CONACYT, Universidad Autónoma de San Luis Potosí,  
San Luis Potosí, 78000, México.*

*e-mail: gabriel.gonzalez@uaslp.mx*

<sup>b</sup>*Coordinación para la Innovación y la Aplicación de la Ciencia y la Tecnología,  
Universidad Autónoma de San Luis Potosí, San Luis Potosí, 78000, México.*

<sup>c</sup>*Instituto Tecnológico de San Luis Potosí,  
Avenida Tecnológico s/n, 78376 Soledad de Graciano Sánchez, SLP, México.*

Received 25 April 2018; accepted 7 June 2018

We present an analogy between the one dimensional Poisson equation in inhomogeneous media, and the Dirac equation in one space dimension with a Lorentz scalar potential for zero energy. We illustrate how the zero energy state in the Jackiw-Rebbi model can be implemented in a simple one dimensional electrostatic setting by using an inhomogeneous electric permittivity and an infinite charged sheet. Our approach provides a novel insight into the Jackiw-Rebbi zero energy state, and provides a helpful way to visualize and teach this important quantum field theory model using basic electrostatics.

*Keywords:* Poisson equation; Dirac equation; Jackiw-Rebbi model.

PACS: 42.25.Bs; 42.82.Et; 42.50.Xa; O3.65.Pm

### 1. Introduction

The Dirac equation is one of the fundamental equations in theoretical physics that accounts fully for special relativity in the context of quantum mechanics for elementary spin-1/2 particles [1]. The Dirac equation plays a key role to many exotic physical phenomena such as graphene, [2] topological insulators [3] and superconductors [4]. These systems proved to be ideal testing grounds for theories of the coexistence of quantum and relativistic effects in condensed matter physics.

Recently, a significant number of studies have addressed the problem of simulating relativistic quantum mechanics using different physical platforms such as optical structures, [5, 6] metamaterials [7] and ion traps [8]. These studies are based on the mathematical analogies found between different physical theories, which provide a way to explore at a macroscopic level many quantum phenomena which are currently inaccessible in microscopic quantum systems. Among the wide variety of quantum-classical analogies investigated so far it appears that the most fruitful one is given by the analogy between optics with quantum phenomena due naturally to the duality between matter and optical waves. The study of quantum-optical analogies is based on the formal similarity between the paraxial optical wave equation in dielectric media and the single particle Schrödinger equation [9]. Among the wide variety of quantum-optical analogies we can mention the Bloch oscillations and Zener tunneling, dynamic localization, Anderson localization, quantum Zeno effect, Rabi flopping and coherent population trapping. All this progress has led to the area of research of how relativistic quantum systems can be mimic by optical waves. More recently, optical systems governed by the relativistic Dirac equation have been investigated experimentally such as Klein Tunneling, Zitterbewegung and the Jackiw-Rebbi model.

The purpose of this article is to demonstrate that electrostatics can provide a laboratory tool where physical phenomena described by the Dirac equation can be explored. In particular, we demonstrate that the Poisson equation in one dimensional inhomogeneous media can be mapped into the zero energy state of the Dirac equation in one dimension with a Lorentz scalar potential. By tailoring the electric permittivity we propose an electrostatic experiment that simulates a historically important relativistic model known as the Jackiw-Rebbi model [10]. Since the derivation of this important model many useful variations of the Jackiw-Rebbi model have been investigated, such as the Ramajaran-Bell model [11], the massive Jackiw-Rebbi model [12], the coupled fermion-kink model [13] and the Jackiw-Rebbi model in distinct kink like backgrounds [14].

The article is organized as follows. First, we will start with a brief review of the Jackiw-Rebbi model and how one can obtain the zero energy state of the JR model. Then we will show how the Poisson equation can be mapped into a Dirac-like equation, and illustrate how the zero energy state in the Jackiw-Rebbi model can be implemented in a simple one dimensional electrostatic setting by using an infinite charged sheet separating two different media. The conclusions are summarized in the last section.

### 2. Jackiw-Rebbi model in one dimension

The Jackiw-Rebbi model describes a one dimensional Dirac field coupled to a static background soliton field, and is known as one of the earliest theoretical description of a topological insulator where the zero energy mode can be understood as the edge state. In particular, the Jackiw-Rebbi model has been studied by Su, Shrieffer and Heeger in the contin-

## Evolutionary Game Theory: A Generalization of the ESS Definition

Elvio Accinelli

*Universidad Autónoma de San Luis Potosí  
Álvaro Obregón #64, Col. Centro, C. P. 78000  
San Luis Potosí, S. L. P., Mexico  
elvio.accinelli@eco.uaslp.mx*

Filipe Martins

*Department of Mathematics, Faculdade de Ciências da  
Universidade do Porto, Rua do Campo  
Alegre, s/n, 4169-007 Porto, Portugal  
Laboratório de Inteligência Artificial e  
Apoio à Decisão (LIAAD), INESC TEC  
Campus da FEUP, Rua Dr. Roberto Frias  
4200-465 Porto, Portugal  
philip-m90@hotmail.com*

Jorge Oviedo\*

*Instituto de Matemática Aplicada San Luis  
Universidad Nacional de San Luis  
Ejército de los Andes 950, 5700 San Luis, Argentina  
Consejo Nacional de Investigaciones  
Científicas y Técnicas (CONICET)  
Ejército de Los Andes 950 5700, San Luis, Argentina  
joviedo@unsl.edu.ar*

Received 3 November 2017

Revised 23 March 2018

Accepted 6 April 2019





Published 28 June 2019

In this paper, we study the concept of Evolutionarily Stable Strategies (ESSs) for symmetric games with  $n \geq 3$  players. The main properties of these games and strategies are analyzed and several examples are provided. We relate the concept of ESS with previous literature and provide a proof of finiteness of ESS in the context of symmetric games with  $n \geq 3$  players. We show that unlike the case of  $n = 2$ , when there are more than two populations an ESS does not have a uniform invasion barrier, or equivalently, it is not equivalent to the strategy performing better against all strategies in a neighborhood.

\*Corresponding author.

## Review Article

# Mechanisms of Resistance to Silver Nanoparticles in Endodontic Bacteria: A Literature Review

Marco Salas-Orozco <sup>1</sup>, Nereyda Niño-Martínez <sup>2</sup>,  
Gabriel-Alejandro Martínez-Castañón <sup>1</sup>, Fernando Torres Méndez,<sup>1</sup>  
Martha Eugenia Compean Jasso,<sup>2</sup> and Facundo Ruiz <sup>2</sup>

<sup>1</sup>Universidad Autónoma de San Luis Potosí, Facultad de Estomatología, C.P. 78000 San Luis Potosí, SLP, Mexico

<sup>2</sup>Universidad Autónoma de San Luis Potosí, Facultad de Ciencias, C.P. 78000 San Luis Potosí, SLP, Mexico

Correspondence should be addressed to Facundo Ruiz; [ruizfacundo1@gmail.com](mailto:ruizfacundo1@gmail.com)

Received 23 August 2018; Revised 12 November 2018; Accepted 29 November 2018; Published 20 January 2019

Academic Editor: Angelo Taglietti

Copyright © 2019 Marco Salas-Orozco et al. This is an open access article distributed under the Creative Commons Attribution License, which permits unrestricted use, distribution, and reproduction in any medium, provided the original work is properly cited.

In recent years, the use and research in nanomaterials have increased considerably. In dentistry, nanomaterials have been investigated in all their specialties like dental prosthesis, implantology, dental operative, periodontics, and endodontics. The nanomaterials are investigated in the areas of dentistry due to their application in the improvement of the physical and chemical properties of conventional materials, as well as the use of the antimicrobial activity of nanomaterials such as silver nanoparticles. Recently, silver nanoparticles (AgNPs) have been studied for their use as an endodontic irrigator due to their high antimicrobial activity. But little is known about the possible mechanisms of the adaptation to AgNPs by endodontic bacteria. These mechanisms may be intrinsic (such as efflux pumps, downregulation of porins, and chromosomal resistance genes) or extrinsic (such as point and adaptive mutations and plasmids with resistance genes) adaptation systems. In addition to this, it has been reported that coselection or coregulation of metal resistance mechanisms, as in the case of nanoparticles, is accompanied by increased resistance to various antibiotics. For these reasons, the objective of this article is to do a review of the literature on the possible mechanisms used by endodontic bacteria to generate resistance to silver nanoparticles and the possible side effects of these mechanisms.

## 1. Introduction

With the emergence of nanotechnology, silver nanoparticles (AgNPs) have been widely used in dentistry, mainly because of their antibacterial properties [1]. They are used in restorative dentistry through their incorporation in composite resins [2] and adhesive systems [3] in order to enhance their mechanical properties and prevent or diminish biofilm accumulation [4]. Silver nanoparticles are studied in dental prostheses where they are incorporated into polymers used as tissue conditioners and as denture bases to prevent the emergence of denture stomatitis. AgNPs are used in implantology to prevent biofilm formation over the implant surface. In endodontics, AgNPs have been incorporated into different materials (root canal sealer, cements, and gutta-percha) to prevent the recolonization of bacteria and have been studied as irrigating solutions and intracanal medication against

bacterial biofilms [5]. This is due to the advantages that AgNPs offer in comparison to sodium hypochlorite (NaOCl). AgNPs maintain their antibacterial efficacy in the presence of dentin [6], and they are used as an alternative to root canal irrigation owing to their biocompatibility, especially in lower concentrations [7]. In addition, studies report that bacteria are not capable of developing resistance to AgNPs compared with antibiotics [8, 9]. Although not all mechanisms are well known, AgNPs can interact simultaneously with multiple targets in the microbial cell, like the cell membrane of both gram-positive and gram-negative bacteria [10, 11], enzymes, proteins [12], lipids [13], DNA, and plasmids [14], making it difficult for bacteria to generate resistance. These mechanisms have already been extensively reviewed [15, 16].

The mechanisms of resistance to silver nanoparticles have not been well studied, but there are reports of silver-resistant bacteria isolated from clinical and nonclinical



# Synthesis and magnetocaloric properties of $\text{La}_{0.67}\text{Ca}_{0.29}\text{Sr}_{0.04}\text{MnO}_3$ obtained from modified sol-gel Pechini method

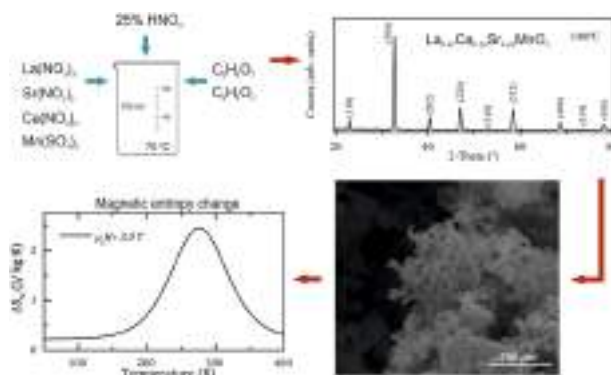
V. E. Salazar-Muñoz<sup>1</sup> · S. A. Palomares-Sánchez<sup>1</sup> · I. Betancourt<sup>2</sup> · T. J. Pérez-Juache<sup>3</sup> · V. D. Compeán-García<sup>4</sup> · A. Lobo Guerrero<sup>5</sup>

Received: 11 January 2019 / Accepted: 25 February 2019  
© Springer Science+Business Media, LLC, part of Springer Nature 2019

## Abstract

This work deals with the study of the physical properties of substituted lanthanum manganite,  $\text{La}_{0.67}\text{Ca}_{0.29}\text{Sr}_{0.04}\text{MnO}_3$ , prepared by using a modified sol-gel Pechini method. The manganite was obtained following the traditional Pechini method, but starting from an unusual mixture of precursors wherein manganese sulfate replaces the manganese nitrate. This single change induces variations on the physical properties of the compound. The phase crystallization was analyzed using X-ray diffraction along with the Rietveld method of refinement of the structure. Morphological analysis showed particle sizes around  $0.5\ \mu\text{m}$  organized in porous structures and forming cubic clusters. The manganite exhibits high crystallinity and second-order ferromagnetic–paramagnetic transition near room temperature. Also, the magnetocaloric effect and the maximum entropy change ( $\Delta S_{M\text{max}}$ ) were calculated by using a phenomenological model. The associated magnetic entropy change  $|\Delta S_M|$  and the relative cooling power have been determined from the phenomenological parameters as a function of the applied magnetic field. In the vicinity of the Curie temperature ( $T_C$ ),  $\Delta S_M$  reached a maximum value of  $2.44\ \text{J/kgK}$  when  $3\ \text{T}$  of magnetic strength was applied.

## Graphical Abstract



✉ A. Lobo Guerrero  
azdlobo@gmail.com

<sup>1</sup> Facultad de Ciencias, Universidad Autónoma de San Luis Potosí, Av. Salvador Nava s/n, 78290 San Luis Potosí, Mexico

<sup>2</sup> Dpto. Materiales Metálicos y Cerámicos, Instituto de Investigaciones en Materiales, Universidad Nacional Autónoma de México, CDMX, Mexico

<sup>3</sup> Escuela Nacional de Estudios Superiores, Universidad Nacional

Autónoma de México, Antigua Carr. Pátzcuaro 8701, 58190 Morelia, Mexico

<sup>4</sup> CONACYT—Coordinación para la Innovación y la Aplicación de la Ciencia y la Tecnología (CIACYT), Universidad Autónoma de San Luis Potosí, Álvaro Obregón 64, 78000 San Luis Potosí, Mexico

<sup>5</sup> Área Académica de Ciencias de la Tierra y Materiales, Universidad Autónoma del Estado de Hidalgo, Carr. Pachuca-Tulancingo Km. 4.5, 42039 Hidalgo, Mexico

## Catalysis

An In Situ Infrared Study of CO<sub>2</sub> Hydrogenation to Formic Acid by Using Rhodium Supported on Titanate Nanotubes as CatalystsJesús Roberto Ruiz-García,<sup>[b]</sup> Juan Carlos Fierro-Gonzalez,<sup>[c]</sup> Brent E. Handy,<sup>[d]</sup> Laura Hinojosa-Reyes,<sup>[a]</sup> David A. De Haro Del Río,<sup>[a]</sup> Carlos J. Lucio-Ortiz,<sup>[a]</sup> Sergio Valle-Cervantes,<sup>[b]</sup> and Gerardo A. Flores-Escamilla<sup>\*[a]</sup>

Titanate nanotubes (TiNT) were synthesized by hydrothermal method and used as support of rhodium nanoparticles. Results of X-Ray diffraction (XRD) and Raman spectroscopy of TiNT revealed its structure of Na<sub>2</sub>Ti<sub>3</sub>O<sub>7</sub>, while the results of Scanning Electron Microscopy (SEM), Transmission Electron Microscopy (TEM) and physisorption of N<sub>2</sub> confirmed the multilayer nanotubular morphology with external diameter of ~12 nm, length > 100 nm and a BET surface area of 195 m<sup>2</sup>g<sup>-1</sup>. The TEM analysis of the rhodium supported sample (Rh/TiNT) showed evidence of small (~1 nm) and highly dispersed rhodium particles. Results of X-Ray Photoelectron Spectroscopy (XPS) revealed a strong electronic interaction between TiNT and Rh

sites. The catalytic activity of Rh/TiNT for the hydrogenation of CO<sub>2</sub> to formic acid at moderate temperature (~40 °C) and atmospheric pressure was demonstrated as evidenced by results of Mass Spectrometry (MS) and *in-situ* Diffuse Reflectance Infrared with Fourier Transform Spectroscopy (DRIFTS). The *in-situ* studies showed active surface species bonded to support sites and to rhodium sites. It is proposed that under H<sub>2</sub> atmosphere, Na<sup>+</sup> cations near to Rh particles promote the conversion of CO<sub>2</sub> via dissociated H, allowing the formation of formate species at low temperature. The formate species and the hydride rhodium complexes are considered reaction intermediates.

## Introduction

Carbon dioxide is a greenhouse gas and it is considered the principal cause of global warming and climate change.<sup>[1,2]</sup> Therefore, several strategies have been evaluated to reduce its concentration in the atmosphere, namely, the introduction of new efficient technologies including the reduction of fossil fuels, the use of perennial energy crops, and increased use of renewable sources (e.g., solar, wind, and geothermal).<sup>[3]</sup> Other alternatives involve effective processes for the capture and sequestration of CO<sub>2</sub>; however, these technologies have high energy requirements.<sup>[1,4]</sup> Therefore, posterior steps that transform the CO<sub>2</sub> into a variety of valuable products are required. A

viable alternative is the utilization of CO<sub>2</sub> as a C1 building block to produce chemicals and fuels. In particular, hydrogenation reactions carried out by homogeneous and heterogeneous catalytic processes<sup>[3-8]</sup> could provide a means for recycling CO<sub>2</sub> emissions. The development of technologies for the use of CO<sub>2</sub> in the production of liquid fuels or energy carriers like methanol, dimethyl ether, and formic acid via catalysis has attracted great research interest in recent years.<sup>[9]</sup>

Formic acid is an important compound utilized in the preparation of silage, the reduction of metallic ions and dyes, tanning leathers, and in the production of esters, allyl alcohol, oxalic acid, and aspartame.<sup>[7,10]</sup> Additionally, the synthesis of formic acid is considered a promising method of hydrogen storage<sup>[8,11]</sup> for its use in fuel cells.<sup>[12,13]</sup> Industrially, formic acid is produced by hydrolysis of methyl formate or formamide and by biomass oxidation.<sup>[9]</sup> However, the separation of formic acid in these processes is complicated and expensive.<sup>[14]</sup> Also, a viable route to obtain formic acid is the hydrogenation of CO<sub>2</sub>, but it must be considered that this reaction is thermodynamically unfavorable ( $\Delta G_{298}^{\circ} = 32.9 \text{ kJ mol}^{-1}$ ).<sup>[15]</sup> This could be overcome using elevated pressures and with the addition of reagents such as alcohols, alkyl halides, and amines to decrease the thermodynamic barrier.<sup>[16,17]</sup> The hydrogenation of CO<sub>2</sub> has been widely studied in homogeneous systems catalyzed by transition-metal as Ru, Rh, Pd, Ir, and Ni.<sup>[4,9,17-22]</sup> The effect of different promoters, ligands, solvents, temperature and pressure conditions have been evaluated.<sup>[4,8,9]</sup> Furthermore, some authors have reported mechanistic details through spectroscopic and kinetic studies.<sup>[7,8,16,17,19-22]</sup> In general, those mecha-

[a] Prof. L. Hinojosa-Reyes, Prof. D. A. De Haro Del Río, Prof. C. J. Lucio-Ortiz, Prof. G. A. Flores-Escamilla  
Universidad Autónoma de Nuevo León, Facultad de Ciencias Químicas, Ave. Universidad s/n, 66455 Nuevo León (México)  
E-mail: gerardo.florescm@uanl.edu.mx

[b] J. R. Ruiz-García, Prof. S. Valle-Cervantes  
Departamento de Ingeniería Química y Bioquímica, Tecnológico Nacional de México, Instituto Tecnológico de Durango, Blvd. Felipe Pescador 1830, 34080 Durango (México)

[c] Prof. J. C. Fierro-Gonzalez  
Departamento de Ingeniería Química, Tecnológico Nacional de México, Instituto Tecnológico de Celaya, Antonio García Cubas 600, 38010 Guanajuato (México)

[d] Prof. B. E. Handy  
CIEP/ Facultad de Ciencias Químicas, Universidad Autónoma de San Luis Potosí, Av. Dr. Manuel Nava 6, 78210 San Luis Potosí (México)

Supporting information for this article is available on the WWW under <https://doi.org/10.1002/slct.201900361>



# Detection of hydroquinone by Raman spectroscopy in patients with melasma before and after treatment

R. Cabrera-Alonso<sup>1</sup> | E. Guevara<sup>1,2</sup> | M. G. Ramírez-Elías<sup>3</sup> | B. Moncada<sup>4</sup> | F. J. González<sup>1</sup>

<sup>1</sup>Terahertz Science and Technology Center (C2T2) and Terahertz Science and Technology National Lab (LANCYTT), Universidad Autónoma de San Luis Potosí, San Luis Potosí, México

<sup>2</sup>CONACYT- Universidad Autónoma de San Luis Potosí, San Luis Potosí, México

<sup>3</sup>Facultad de Ciencias, Universidad Autónoma de San Luis Potosí, San Luis Potosí, México

<sup>4</sup>Dermatology Department, Hospital Central 'Dr. Ignacio Morones Prieto', Universidad Autónoma de San Luis Potosí, San Luis Potosí, México

## Correspondence

E. Guevara, CONACYT-Universidad Autónoma de San Luis Potosí, San Luis Potosí, México.  
Email: edgar.guevara@uaslp.mx

## Funding information

Dermatology Department of the Hospital Central 'Dr. Ignacio Morones Prieto'; Consejo Nacional de Ciencia y Tecnología, Grant/Award Number: Doctoral Grant and Project 528 Cátedras; Terahertz Science and Technology National Lab (LANCYTT)

## Abstract

**Background:** Melasma is an acquired, facial hyperpigmentation without a specific origin. It is regularly associated with multiple etiologic factors such as pregnancy, genetic, racial, and from estrogen administration. Among the methods to treat skin hyperpigmentation a series of skin bleaching agents have been used. At present, the most commonly used agent is known as hydroquinone. Nowadays, it is known that hydroquinone can cause cancer in animals with unknown relevance to humans.

**Material and Methods:** In this work, Raman spectroscopy was used to observe the presence of hydroquinone in the skin of 18 patients who have been under treatment for melasma.

**Results:** A significant increase in the Raman signal was observed in the six bands associated with hydroquinone after melasma treatment.

**Conclusion:** The authors believe that monitoring the presence of hydroquinone may be useful for an optimal personalized treatment of melasma and to provide the specialist a support tool to control the administration of this type of bleaching agents.

## KEYWORDS

hydroquinone, melasma, non-invasive diagnostics, Raman spectroscopy

## 1 | INTRODUCTION

Hydroquinone is an aromatic compound in the form of light tan to gray crystals. It is used as a skin bleaching agent, in cosmetics, hair dye, glue, and as medication to treat melasma. Hydroquinone is biodegradable but can be toxic to microorganisms at high concentrations.<sup>1</sup> People using commercial skin lighteners containing hydroquinone developed a blue- or brownish-blue-colored skin. Effects on the kidney, liver, and forestomach, including cancer, were found in laboratory rats fed hydroquinone in the diet or in water.<sup>1</sup> In 1999, the International Agency for Research on Cancer determined that hydroquinone did not possess carcinogenic properties in humans. This decision was based on limited data in animal models and lack of evidence in humans. In 2014, the American Conference

of Governmental Industrial Hygienists decided that hydroquinone is confirmed to cause cancer in animals with unknown relevance to humans, although a 2 mg/m<sup>3</sup> exposure guideline was recommended per workshift<sup>1</sup>. This compound has not endured a full assessment under the US EPA's IRIS (Integrated Risk Information System, prepared and maintained by the Environmental Protection Agency of the United States of America) program for evidence of cancer risk to humans.<sup>1</sup>

Nevertheless, monitoring the presence of this substance at high concentrations in the skin of patients who have been under clinical lightening treatments for melasma could be useful for future carcinogenesis studies. These days, critical innovative advances have been accomplished at the intersection of scientific and technological fields, such as optics, materials science, medicine and electronics.





# Use of Raman spectroscopy in the assessment of skin after CO<sub>2</sub> ablative fractional laser surgery on acne scars

Fernando Sebastian Chiwo<sup>1</sup> | Edgar Guevara<sup>1,2</sup> | Miguel Ghebre Ramirez-Elías<sup>3</sup> |  
Claudio Cayetano Castillo-Martínez<sup>4</sup> | Carlos Eduardo Osornio-Martínez<sup>1</sup> |  
Rodrigo Cabrera-Alonso<sup>1</sup> | Francisco Pérez-Atamoros<sup>5</sup> | Francisco Javier González<sup>1</sup>

<sup>1</sup>Terahertz Science and Technology Center (C2T2) and Terahertz Science and Technology National Laboratory (LANCYTT), Universidad Autónoma de San Luis Potosí, San Luis Potosí, México

<sup>2</sup>CONACYT, Universidad Autónoma de San Luis Potosí, San Luis Potosí, México

<sup>3</sup>Facultad de Ciencias, Universidad Autónoma de San Luis Potosí, San Luis Potosí, México

<sup>4</sup>Hospital "Lomas de San Luis", San Luis Potosí, México

<sup>5</sup>Centro Dermatológico Tennyson, México D.F., México

## Correspondence

Fernando Sebastian Chiwo, Terahertz Science and Technology Center (C2T2) and Terahertz Science and Technology National Laboratory (LANCYTT), Universidad Autónoma de San Luis Potosí, Av. Sierra Leona 550, Lomas 2a. Secc., 78210, San Luis Potosí, México.  
Email: sebastian.chiwo@gmail.com

## Funding information

Catedras CONACYT, Grant/Award Number: No. 528; CONACYT National Labs, Grant/Award Number: Terahertz Science and Technology National Laboratory; Centro Mexicano de Innovación en Energía Solar, Grant/Award Number: 105; CONACYT, Grant/Award Number: Scholarship No. 559382

## Abstract

**Background:** Ablative fractional laser surgery is a common technique for treating acne scars. However, an in vivo and noninvasive analysis of the histologic variations between acne skin and the resulting resurfaced skin is needed in order to evaluate the wound healing process of the scars induced by the ablative fractional laser surgery.

**Materials and Methods:** Nine patients with acne scars underwent a single treatment with a CO<sub>2</sub> ablative fractional laser surgery. Collagen presence on the resurfaced skin was noninvasively assessed by means of Raman spectroscopy and principal component analysis.

**Results:** Principal component analysis shows that all the patients presented a collagen regeneration on the resurfaced skin after the laser treatment.

**Conclusion:** Collagen plays a crucial role in the wound healing process. By assessing the collagen presence on the skin, it was possible to quantify the regenerative effects of the ablative fractional laser in a noninvasive way.

## KEYWORDS

collagen, laser surgery, Raman spectroscopy, skin resurfacing

## 1 | INTRODUCTION

Acne is a skin disease with chronic and inflammatory characteristics that is present on the pilosebaceous unit appearing first at puberty and often in adulthood. Its pathophysiology involves hyperseborrhea, non-normal follicular-based keratinization, and Propionibacterium acnes increase in the pilosebaceous unit resulting in a change in the cutaneous microenvironment leading to inflammatory reactions.<sup>1</sup>

Ablative fractional laser (AFL) surgery is widely used in the medical field because it is able to reduce trauma due to the short-time exposure to radiation.<sup>2</sup> Isotretinoin has been considered for several decades the gold standard for nodulocystic acne or inflammatory acne, which has failed other course treatments, due to its anti-inflammatory properties.<sup>3</sup> It has been established that combining the use of AFL surgery with oral isotretinoin improvement is observed on acne scars in a short period of time with no acne relapse or adverse effects over the resurfaced skin.<sup>4-8</sup>



# Effect of H bonds on thermal behavior and cohesion in polylactic acid nanocomposites and nitrogen-doped carbon nanotubes

I. Montes-Zavala<sup>1</sup> , E. O. Castrejón-González<sup>1,\*</sup> , G. Sánchez-Balderas<sup>2</sup> ,  
E. Pérez<sup>2</sup> , and J. A. González-Calderón<sup>3,\*</sup>

<sup>1</sup>Departamento de Ingeniería Química, Tecnológico Nacional de México en Celaya, Av. Tecnológico y A. García Cubas S/N, 38010 Celaya, Guanajuato, Mexico

<sup>2</sup>Instituto de Física, Universidad Autónoma de San Luis Potosí, Av. Manuel Nava #6, Zona Universitaria, 78290 San Luis Potosí, San Luis Potosí, Mexico

<sup>3</sup>Cátedras CONACYT-Instituto de Física, Universidad Autónoma de San Luis Potosí, Av. Manuel Nava #6, Zona Universitaria, 78290 San Luis Potosí, San Luis Potosí, Mexico

Received: 28 August 2019

Accepted: 21 November 2019

© Springer Science+Business Media, LLC, part of Springer Nature 2019

## ABSTRACT

In this work, we explain the filling effect of pristine carbon nanotubes (CNTs) and nitrogen-doped carbon nanotubes (N-CNTs) under the properties of polylactic acid (PLA) nanocomposites by combining molecular dynamics simulations and experimental results. We observed via computational analysis that the presence of nitrogen in the CNTs improves their integration with the polymer chains. An experimental study of these systems showed that the addition of N-CNT in the PLA matrix causes different phenomena: The PLA crystallinity decreases, crystalline domains form at the surface of the composites due to nanostructure doping, and the energy dissipates by an order of magnitude. In addition, the glass transition and melting temperatures of the PLA nanocomposites were calculated by molecular dynamics simulations, which were in good agreement with the obtained experimental results. The computational study also revealed a good integration of N-CNTs with PLA chains due to the generation of strong hydrogen bonds between the nanotubes and the polymer chains. This last result was also confirmed by the PLA radius of gyration and by the radial distribution function of C–H and N–H pairs between the nanotube and polymer, both indicating an approach of the polylactic acid chains toward doped carbon nanotubes.

Address correspondence to E-mail: amir@ifisica.uaslp.mx; omar@iqcelaya.itc.mx



## RESEARCH ARTICLE

# Near-field analysis of discrete bowtie plasmonic nanoantennas

Camilo Moreno<sup>1</sup> Javier Méndez-Lozoya<sup>2</sup> |Gabriel González<sup>2</sup> |Francisco J. González<sup>2</sup> |Glenn Boreman<sup>1</sup>

<sup>1</sup>Physics and Optical Science Department, University of North Carolina at Charlotte, Charlotte, North Carolina

<sup>2</sup>LANCYTT – Terahertz National Lab, Universidad Autónoma de San Luis Potosí, San Luis Potosí, Mexico

**Correspondence**

Camilo Moreno, Physics and Optical Science Department, University of North Carolina at Charlotte, Charlotte, NC 28223.

Email: cmorenoc@uncc.edu

**Funding information**

Consejo Nacional de Ciencia y Tecnología (CONACyT) - Mexico, Grant/Award Number: CEMIE-Sol 32; Terahertz Science and Technology National Lab

**Abstract**

A discrete antenna is a discretized version of a traditional antenna design which enhances the antenna properties (such as field intensity, multi-band, compact size, and low sidelobe levels) of its traditional counterpart. In this work, a classical bowtie antenna is discretized using circular elements of different sizes. Numerical simulations and near-field optical scanning microscopy are performed on classical and discrete bowtie antennas in the infrared. Simulations show that discrete antennas have an increased bandwidth and an increased number of electric-field hotspots and near-field measurements confirm the increment of hotspots. These characteristics make discrete antennas potentially useful in applications where an extended region of localized electric field enhancements is of interest.

**KEYWORDS**

discrete bowtie, plasmonic nanoantenna, scanning-scattering near-field optical microscopy

**1 | INTRODUCTION**

In recent decades the use of plasmonic antennas has attracted attention due to the electric field enhancement in sub-wavelength regions which has potential applications in nanolithography, biosensing, and optical imaging.<sup>1-6</sup> Implementation of plasmonic antennas has been accomplished by adapting the designs from radio-frequency and microwave counterparts and redesigning them for the infrared (IR) and optical frequencies.<sup>1</sup> These designs range from microstrip dipoles, bowtie antennas, spiral antennas, diablo antennas to antenna arrays.<sup>6-9</sup> In particular, bowtie antennas are a realistic and practical approximation of the biconical antenna. Bowtie antennas consist of two triangles with a gap between the vertices. However, a bowtie antenna is narrowband compared with the biconical antenna.<sup>10</sup> Geometrical modifications to the bowtie design have been proposed to improve the antenna bandwidth in the radio spectrum, at the expense of larger antenna area or the implementation of rounded corners.<sup>11</sup> When extending these ideas to the optical and IR frequencies, numerical simulations and experiments of plasmonic bowtie antennas have shown that localized field intensity is enhanced.<sup>12-14</sup> Optical bowtie nanoantennas generate a strong field enhancement at the gap of the antenna due to surface-plasmon currents generated in the antenna arms combined with a strong capacitive coupling at the gap of the antenna.<sup>12</sup> Because of this feature bowtie nanoantennas have been applied for sensing applications such as surface-enhanced Raman spectroscopy,<sup>15</sup> improving the fluorescence emission in biosensing and subwavelength imaging.<sup>16,17</sup>

The discrete bowtie antenna we study in the present work is based on the traditional bowtie antenna design, where discrete elements are used in order to increase the field enhancement near the antenna and to widen its frequency response.<sup>18</sup> The performance of discrete bowtie plasmonic nanoantennas is investigated and compared to classic bowtie antennas.

**2 | MATERIALS AND METHODS**

Classical bowtie antennas and discrete bowtie antennas were fabricated using electron beam lithography on silicon substrates and their electric-field enhancement was investigated using a scanning-scattering near-field optical microscope (s-SNOM) and also by finite-element simulations,



Article

# Detection of Histamine Dihydrochloride at Low Concentrations Using Raman Spectroscopy Enhanced by Gold Nanostars Colloids

Eleazar Samuel Kolosovas-Machuca <sup>1</sup>, Alexander Cuadrado <sup>1,2</sup>, Hiram Joazet Ojeda-Galván <sup>1,3</sup> , Luis Carlos Ortiz-Dosal <sup>4</sup>, Aida Catalina Hernández-Arteaga <sup>1</sup>, Maria del Carmen Rodríguez-Aranda <sup>1</sup>, Hugo Ricardo Navarro-Contreras <sup>1</sup>, Javier Alda <sup>2,\*</sup> and Francisco Javier González <sup>1</sup>

<sup>1</sup> Coordinación para la Innovación y Aplicación de la Ciencia y la Tecnología, Universidad Autónoma de San Luis Potosí, 78210 San Luis Potosí, Mexico; samuel.kolosovas@uaslp.mx (E.S.K.-M.); a.cuadrado@pdi.ucm.es (A.C.); joazet.ojeda@uaslp.mx (H.J.O.-G.); aida.arteaga@uaslp.mx (A.C.H.-A.); carmen.rgz.aranda@gmail.com (M.d.C.R.-A.); hnavarro@uaslp.mx (H.R.N.-C.); javier.gonzalez@uaslp.mx (F.J.G.)

<sup>2</sup> Applied Optics Complutense Group, Faculty of Optics and Optometry, University Complutense of Madrid, Av. Arcos de Jalon, 118, 28037 Madrid, Spain

<sup>3</sup> Instituto de Física Luis Terrazas, Benemerita Universidad Autónoma de Puebla, Av. San Claudio, 18, 72570 Puebla, Mexico

<sup>4</sup> Doctorado Institucional en Ingeniería y Ciencias de Materiales, Universidad Autónoma de San Luis Potosí, 78210 San Luis Potosí, Mexico; ortiz.dosal.lc@gmail.com

\* Correspondence: javier.alda@ucm.es; Tel.: +34-91-394-6874

Received: 20 December 2018; Accepted: 22 January 2019; Published: 6 February 2019



**Abstract:** In this paper, we report a fast and easy method to detect histamine dihydrochloride using gold nanostars in colloidal aqueous solution as a highly active SERS platform with potential applications in biomedicine and food science. This colloid was characterized with SEM and UV–Vis spectroscopy. Also, numerical calculations were performed to estimate the plasmonic resonance and electric field amplification of the gold nanoparticles to compare the difference between nanospheres and nanostars. Finally, aqueous solutions of histamine dihydrochloride were prepared in a wide range of concentrations and the colloid was added to carry out SERS. We found SERS amplified the Raman signal of histamine by an enhancement factor of  $1.0 \times 10^7$ , demonstrating the capability of the method to detect low concentrations of this amine molecule.

**Keywords:** SERS; histamine; nanostars; nanophotonics; computational electromagnetism

## 1. Introduction

Surface-enhanced Raman spectroscopy (SERS) is a useful technique for the characterization of small groups of molecules near or bound to plasmonic surfaces. It is powerful, non-destructive, and provides information about the chemical structure and identity of materials [1–5]. These capabilities make possible the wide use of SERS in biosensors for the detection of substances of biological interest and pathogens [5–11], being gold and silver two of the metals that offer better results for this kind of applications [12–15]. The above-mentioned metals in the form of nanoparticles have the advantage that can be used directly, as colloidal solutions, acting as tridimensional plasmonic systems with customized resonances that can be tuned with the size and shape of the dispersed nanoparticles [4,16,17]. Au nanostars have been proven useful for SERS, they also present unique optical and electric properties. Previous groups have reported the synthesis of Au nanostar with



Cite this: DOI: 10.1039/c9ce00104b

## Orthorhombic distortion in Au nanoparticles induced by high pressure

Rubén Mendoza-Cruz,<sup>id</sup>\*<sup>ab</sup> Prakash Parajuli,<sup>a</sup> H. Joazet Ojeda-Galván,<sup>id</sup><sup>cd</sup> Ángel Gabriel Rodríguez,<sup>c</sup> Hugo R. Navarro-Contreras,<sup>id</sup><sup>c</sup> J. Jesús Velázquez-Salazar,<sup>a</sup> Lourdes Bazán-Díaz,<sup>id</sup><sup>ab</sup> and Miguel José-Yacamán<sup>a</sup>

It is well known that the properties of metal nanoparticles strongly depend on their size. This dependence can generate unusual structures, and it enabled induction of phase transitions at lower pressure and temperature compared to the bulk materials. Bulk transition metals do not have phase transitions under ambient conditions. Bulk gold phase transitions are expected at pressures above 200 GPa. Herein, it is reported that an orthorhombic lattice distortion in single-crystal truncated-octahedral gold nanoparticles is induced by applying a high pressure below 12 GPa in a diamond anvil cell at room temperature (295 K). An asymmetrical lattice distortion of ~3% along the lattice planes, detected through atomic-resolution electron microscopy and electron diffraction, indicated that lattice strain generated by the imposed experimental conditions led to a transition from a cubic to an orthorhombic structure. Interestingly, the mentioned lattice distortion was not observed in twinned nanoparticles subjected to the same pressure and temperature conditions. The lattice deformation took place at a much lower pressure and temperature compared to that of bulk gold, demonstrating dependency on the particle shape and structure. The experimental results reflect not only a size effect, but also a strong surface, morphological, and structural effect on the behavior of materials at the nanoscale under high-pressure conditions.

Received 20th January 2019,  
Accepted 28th April 2019

DOI: 10.1039/c9ce00104b

rsc.li/crystengcomm

### 1. Introduction

The importance in engineering applications of the behavior of materials under high pressure has promoted the recent development in the research field of high-density materials, where the appearance of different nanophases is usually involved.<sup>1,2</sup> Gold, the noblest of all metals, presents great stability, biocompatibility, and chemical inertness that have been used in countless applications,<sup>3–6</sup> as well as a pressure standard in high-pressure experiments, owing to its low strength, moderate compressibility, and X-ray and electron scattering power.<sup>7,8</sup> However, size and surface effects have generated unexpected structural transitions in nanoparticles at pressures and temperatures not expected in their bulk counterparts, generating unusual structures in different metal nanoparticles.<sup>9–11</sup> Despite extensive studies, the mechanical properties of nanoparticles as a

function of size are still not well understood because of inconsistent results on the size-dependence of the bulk modulus.

Bulk transition metals do not have phase transitions under ambient conditions. A phase transition of gold is expected at very high pressure. Different experimental and theoretical studies have been performed to calculate and describe the possible phase transitions in bulk gold, usually focused on face-centered cubic (FCC) to hexagonal-closed packed (HCP) structural transitions<sup>12–14</sup> or a body-centered cubic transition.<sup>15</sup> All of these transitions occur at pressures above at least 200 GPa.

Notwithstanding, at the nanoscale, a drastic change in the mechanical properties of different FCC metallic nanoparticles has been observed with decreasing particle size. The great advance in the determination of the effects of particle size on the mechanical properties of nanomaterials has been associated with the development of *in situ* diamond anvil cells (DAC), enabling the progress in high-pressure science.<sup>16–19</sup> Through high-pressure experiments, metal nanoparticles have been proved to exhibit enhanced mechanical properties when particle size decreases. A reduction of the interatomic distances up to 10 GPa in gold nanoparticles,<sup>20</sup> an increase of the strength in 30 nm Au nanoparticles up to 60 GPa compared to the bulk,<sup>21</sup> a high stiffness of Ag and Au nanoparticles at a pressure up to ~30 GPa,<sup>22</sup> the enhancement of

<sup>a</sup> Department of Physics & Astronomy, University of Texas at San Antonio, One UTSA Circle, San Antonio, TX 78249, USA. E-mail: ruben.mendozacruz@utsa.edu

<sup>b</sup> Department of Chemical and Biomedical Engineering, University of Texas at San Antonio, One UTSA Circle, San Antonio, TX 78249, USA


<sup>c</sup> Coordinación para la Innovación y la Aplicación de la Ciencia y la Tecnología (CIACYT), Universidad Autónoma de San Luis Potosí (UASLP), Álvaro Obregón 64, 78000 San Luis Potosí, Mexico

<sup>d</sup> Instituto de Física, Luis Rivera Terrazas, Benemérita Universidad Autónoma de Puebla. Av. San Manuel, Ciudad Universitaria, Puebla, Pue. 72570, México

# Differential reflectance contrast technique in near field limit: Application to graphene

Cite as: AIP Advances 9, 045309 (2019); <https://doi.org/10.1063/1.5092339>

Submitted: 10 February 2019 . Accepted: 29 March 2019 . Published Online: 10 April 2019

L. F. Lastras-Martínez , D. Medina-Escobedo, G. Flores-Rangel, R. E. Balderas-Navarro, O. Ruiz-Cigarrillo, R. Castro-García , M. del P. Morales-Morelos, J. Ortega-Gallegos, and M. Losurdo



View Online



Export Online



CrossMark

AVS Quantum Science

Co-published with AIP Publishing



Coming Soon!



## Research Article

# Detection of Genes Related to Resistance to Silver Nanoparticles in Bacteria from Secondary Endodontic Infections

Marco Felipe Salas-Orozco <sup>1</sup>, Nereyda Niño Martínez <sup>2</sup>,  
Gabriel-Alejandro Martínez-Castañón <sup>2</sup>, Fernando Torres Méndez,<sup>1</sup> Nuria Patiño-Marín,<sup>1</sup>  
and Facundo Ruiz <sup>2</sup>

<sup>1</sup>Facultad de Estomatología, Universidad Autónoma de San Luis Potosí, San Luis Potosí, Mexico

<sup>2</sup>Facultad de Ciencias, Universidad Autónoma de San Luis Potosí, San Luis Potosí, Mexico

Correspondence should be addressed to Nereyda Niño Martínez; [nereyda.nino@uaslp.mx](mailto:nereyda.nino@uaslp.mx)

Received 1 April 2019; Revised 19 July 2019; Accepted 20 August 2019; Published 12 September 2019

Academic Editor: Andrew R. Barron

Copyright © 2019 Marco Felipe Salas-Orozco et al. This is an open access article distributed under the Creative Commons Attribution License, which permits unrestricted use, distribution, and reproduction in any medium, provided the original work is properly cited.

**Introduction.** Silver nanoparticles are used in endodontics due to their antimicrobial activity, although it is considered that bacteria are unable to develop resistance to silver nanoparticles. Silver resistance genes have been related to resistance to nanoparticles and antibiotics. The presence of these resistance genes has not been studied in endodontic bacteria. The objective of this study is to report the prevalence of silver resistance genes in endodontic bacteria. **Methods.** The selected teeth were isolated using a rubber dam and any restoration, post, or caries was eliminated. The operative field was disinfected, and the root-filling material was removed. The samples were obtained using three sterile paper points to absorb the fluid of the root canal. The DNA from the samples and the control organism was extracted, and the detection of the *silCBA* resistance genes was carried out by PCR. **Results.** The results of this study show a high prevalence (73.3%) of *silCBA* silver resistance genes. The Spearman rank correlation coefficient was utilized to identify correlations between the presence of genes and clinical variables. **Conclusions.** This study reports a high frequency of silver resistance genes related to nanoparticle resistant from bacteria.

## 1. Introduction

Nanoparticles (NPs) have been widely used in various areas of dentistry, mainly due to their potent antibacterial property [1]. In endodontics, silver nanoparticles (AgNPs) are used to combat the presence of biofilms [2]. This is because AgNPs have several advantages compared to NaOCl (the gold standard of disinfection in endodontics). AgNPs can retain their antibacterial efficacy in the presence of dentine and have greater biocompatibility, especially at low concentrations [3].

In general, it is mentioned that silver nanoparticles exert their bactericidal action through two mechanisms. The first mechanism consists of the direct penetration of the nanoparticle (<10 nm) into the bacterial cell, and the second is the release of silver ions (by nanoparticles > 10 nm) that can also enter the bacterial cells and react with their components causing the death of the bacteria. Although it is thought that

bacteria are not capable of developing resistance to silver nanoparticles, this has not been well studied, although silver-resistant bacteria isolated from clinical and nonclinical environments have been reported [4, 5]. The first clinical bacterium with silver resistance described was *Salmonella typhimurium*. The first plasmid coding for bacterial resistance to Ag<sup>+</sup> was isolated from this bacterium. The plasmid was named pMG101, and it confers resistance to Ag<sup>+</sup>, Hg<sup>+</sup>, and tellurite as well as antibiotics, such as ampicillin, chloramphenicol, tetracycline, and streptomycin. This plasmid contains a region of 14.2 kb (*sil operon*) with nine ORFs (open reading frames) arranged in three transcriptional units (*silCFBAGP*, *silRS*, and *silE*) expressed from a different promoter. These transcriptional subunits are collectively designated as the *Sil operon* [6]. The first transcriptional unit is composed of *silCFBAGP*. This transcription unit encodes an internal membrane protein complex formed by three

## RESEARCH ARTICLE

# Temperature dependence of the Raman dispersion of Sr<sub>2</sub>Nb<sub>2</sub>O<sub>7</sub>: Influence of an electric field during the synthesis

Javier Alanis<sup>1</sup>  | M. C. Rodríguez-Aranda<sup>2</sup>  | Ángel G. Rodríguez<sup>2</sup>  |Hiram Joazet Ojeda-Galván<sup>1,2</sup>  | María Eugenia Mendoza<sup>1</sup>  | Hugo R. Navarro-Contreras<sup>2</sup> 

<sup>1</sup>Instituto de Física, Luis Rivera Terrazas, Benemérita Universidad Autónoma de Puebla, Av. San Claudio and Boulevard 18 Sur, Col. San Manuel, Ciudad Universitaria, Puebla, Pue. 72570, Mexico

<sup>2</sup>Coordinación para la Innovación y Aplicación de la Ciencia y la Tecnología (CIACYT), Universidad Autónoma de San Luis Potosí, Álvaro Obregón 64, San Luis Potosí, S.L.P. 78000, Mexico

**Correspondence**

Hiram Joazet Ojeda-Galván and Hugo R. Navarro-Contreras, Coordinación para la Innovación y Aplicación de la Ciencia y la Tecnología (CIACYT), Universidad Autónoma de San Luis Potosí, Álvaro Obregón 64, San Luis Potosí 78000, Mexico.

Email: joazet.ojeda@uaslp.mx; hnavarro@uaslp.mx

**Funding information**

Consejo Nacional de Ciencia y Tecnología, Grant/Award Numbers: CEMIESOL/ 22, Ciencia Básica/ 256788 Problemas nacionales/ 2015-01-986; CONACYT Network of National Laboratories; Laboratorio Nacional de Supercomputo del Sureste de México; Consejo Nacional de Ciencia y Tecnología (CONACYT) México

**Abstract**

We report on the preparation and structural characterization of powder samples of the perovskite-slab layered polycrystalline Sr<sub>2</sub>Nb<sub>2</sub>O<sub>7</sub> (hereafter named SNO) ferroelectric compound. Comparison is performed on samples grown without (SNO) and with an applied electric field of 3.34 kV/cm (SNOE). The Raman effect produced by these samples as a function of temperature, from 27°C (room temperature) to 400°C is presented and discussed. Significant differences are observed and discussed among SNO and SNOE. The electric field promotes the growth of platelets, preferentially oriented along the (0b0) planes. The temperature coefficients of 35 phonon wavenumbers were determined for both samples. A majority of the phonons exhibit monotonic wavenumber softening's with increasing temperatures, but a significant number of them show discontinuities on the wavenumber temperature slopes at two temperatures 215°C and 307 ± 5°C. The first temperature corresponds to the well-known incommensurate phase to the ferroelectric phase transition (Phases III to II). The second temperature is indicative of an unreported phase transition for both the SNO and SNOE samples. For the sample SNOE, a phonon f7 (at 121 cm<sup>-1</sup> at room temperature) displays a behavior that may be indicative of the existence of another ordering parameter that vanishes at 488 ± 5°C in the SNOE sample, induced by the electric field applied during the growth. The phonon broadenings with temperature are explained in terms of the Klemens model, which considers that the broadenings are due to the thermal expansion of the lattice, with a substantial contribution in magnitude from anharmonic phonon-phonon interactions.

**KEYWORDS**

ferroelectric, layered perovskite, phase transitions, Sr<sub>2</sub>Nb<sub>2</sub>O<sub>7</sub>, XRD versus temperature

## 1 | INTRODUCTION

Strontium (Pyro)Niobate Sr<sub>2</sub>Nb<sub>2</sub>O<sub>7</sub> (SNO) is a layered perovskite compound, that belongs to a set of complex layered compounds that have the chemical composition<sup>[1]</sup> Sr<sub>n</sub>Nb<sub>n</sub>O<sub>3n + 2</sub>. Here, *n* indicates the number of NbO<sub>6</sub>

octahedra (*n* = 4, for Sr<sub>2</sub>Nb<sub>2</sub>O<sub>7</sub>), composing the slab thickness. The SrNbO<sub>3</sub> slabs are stacked along the *b*-axis of the orthorhombic phase adopted at room temperature.<sup>[2]</sup> Recently, this compound has attracted interest as a ferroelectric insulator,<sup>[3]</sup> as a ferroelectric memory field effect transistor,<sup>[4]</sup> for its interesting thermoelectric





ORIGINAL ARTICLE

# Determination of Salivary Sialic Acid Through Nanotechnology: A Useful Biomarker for the Screening of Breast Cancer

Aida Catalina Hernández-Arteaga,<sup>a</sup> José de Jesús Zermeño-Nava,<sup>b</sup> Marco Ulises Martínez-Martínez,<sup>b,c</sup>  
Alondra Hernández-Cedillo,<sup>a</sup> Hiram Joazet Ojeda-Galván,<sup>a,d</sup> Miguel José-Yacamán,<sup>a,e</sup> and  
Hugo Ricardo Navarro-Contreras<sup>a</sup>

<sup>a</sup>Coordinación para la Innovación y Aplicación de la Ciencia y la Tecnología (CIACYT), Universidad Autónoma de San Luis Potosí, San Luis Potosí, Mexico

<sup>b</sup>División de Gineco-Obstetricia, Hospital Central Dr. Ignacio Morones Prieto, San Luis Potosí, Mexico

<sup>c</sup>Hospital General de Zona 1, Instituto Mexicano del Seguro Social, San Luis Potosí, Mexico

<sup>d</sup>Instituto de Física, Luis Rivera Terrazas, Benemérita Universidad Autónoma de Puebla, Puebla, México

<sup>e</sup>Department of Physics and Astronomy, University of Texas at San Antonio, San Antonio, TX, USA

Received for publication March 22, 2019; accepted May 30, 2019 (ARCMED\_2019\_254).

Available online xxx

**Purpose.** To demonstrate the usefulness of sialic acid (SA) in saliva as a biomarker for breast cancer (BC) and develop a new tool for early detection.

**Methods.** Considering that the amount of SA in human saliva is limited, the levels of SA were measured using surface-enhanced Raman spectroscopy (SERS) with tailored citrate-reduced silver nanoparticles. We calibrated the spectrum using analytical reagent SA. The 164 patients included in this study were undergoing screening mammography and/or ultrasound testing. The SA test was performed in the absence of previous information regarding the health of the subjects. Biopsies were performed to determine the diagnosis of cancer condition. The biopsy studies determined that 35 patients are BC affected and 129 gave negative results.

**Results.** SERS showed a sensitivity and specificity of 80 and 93%, respectively. The cut-off value for SA (12.5 mg/dL) was established through a receiver operating characteristic (ROC) curve analysis. The area under the curve of the ROC analysis resulted in 95% with this SA level cut-off. Our results suggest that SA may be a useful biomarker for the screening of breast cancer in women.

**Conclusions.** Our results suggest that the SA levels measured from saliva may be highly sensitive and specific markers for the presence of breast cancer. © 2019 IMSS. Published by Elsevier Inc.

**Key Words:** Breast cancer, Biomarkers, Surface-enhanced Raman, Ag nanoparticles, Nanotechnology.

## Introduction

Breast cancer (BC) is the most frequent malignancy in females, responsible for more than 520,000 deaths per year worldwide. It is the second leading cause of death due to cancer in females, surpassed only by lung cancer (1). Early detection of BC at clinically undetectable stages, combined with aggressive and prompt medical intervention, is

essential to substantially reduce the mortality rates associated with this malignancy. It has been established that screening for BC complies with the Wilson and Jungner screening criteria and has resulted in reductions in mortality by > 20%, and in a mean survival time of 15.8 years (2,3).

The preferred techniques for BC screening are mammography and ultrasound in subjects with fibrous breast tissue. However, both techniques are limited by the operator-dependent interpretation of the results (4). Despite this limitation, technological advancements and carefully executed screening programs can result in important reductions in the mortality rate of BC (2,3). Mammography is linked to a slightly increased risk of radiation-induced BC (3). Thus,

Address reprint requests to: Hiram Joazet Ojeda-Galván, Coordinación para la Innovación y Aplicación de la Ciencia y la Tecnología (CIACYT), Universidad Autónoma de San Luis Potosí, Álvaro Obregón 64, San Luis Potosí 78000, Mexico; Phone: 011524448262300; E-mail: joazet.ojeda@uaslp.mx



# Use of Raman spectroscopy to screen diabetes mellitus with machine learning tools: reply to comment

EDGAR GUEVARA,<sup>1,2,\*</sup>  JUAN CARLOS TORRES-GALVÁN,<sup>2</sup> MIGUEL G. RAMÍREZ-ELÍAS,<sup>3</sup> CLAUDIA LUEVANO-CONTRERAS,<sup>4</sup> AND FRANCISCO JAVIER GONZÁLEZ<sup>2</sup> 

<sup>1</sup>CONACYT-Universidad Autónoma de San Luis Potosí, Mexico

<sup>2</sup>Terahertz Science and Technology Center (C2T2) and Science and Technology National Lab (LANCyTT), Universidad Autónoma de San Luis Potosí, Mexico

<sup>3</sup>Facultad de Ciencias, Universidad Autónoma de San Luis Potosí, Mexico

<sup>4</sup>Department of Medical Sciences, University of Guanajuato, Leon, Mexico

\*[eguevara@conacyt.mx](mailto:eguevara@conacyt.mx)

**Abstract:** We show the spectra of advanced glycation products in response to recent comments made by Bratchenko *et al.* Our results suggest that information retrieved by Raman spectroscopy is relevant to screening diabetic patients, however, the comparison carried out in our paper, between ANN and SVM, was not fair, because of the erroneous PCA selection procedure and different sources of variation present in the analysis.

© 2019 Optical Society of America under the terms of the [OSA Open Access Publishing Agreement](#)

## 1. Reply

We thank Bratchenko *et al.* [1] for their critical comment to our paper [2]. Indeed, there was a miscalculation of the spot size, which was stated to be 200 $\mu\text{m}$ , but it was approximately 4mm. However, this spot size refers to the  $1/e^2$  width, which leads to an effective irradiance of 1.45 W/cm<sup>2</sup>, well within the ANSI standard. Furthermore, none of the patients showed signs of pain, numbness, tingling or discomfort during the Raman spectroscopy measurements and there were no visible signs of the slightest irritation on the acquisition sites.

We need to clarify that the standard deviations depicted in Fig. 1 of our previous work [2] were computed from the averaged spectra of eleven diabetic patients and nine controls respectively.

Regarding the possible overfitting of our artificial neural network (ANN), it is mentioned in our work that “all metrics of performance reported in this paper were computed by averaging the results of one thousand 10-fold cross-validation runs”, this was done precisely in order to take into account large difference in variance between the test set and the training set. Moreover, our runs showed that the classifier achieved a low training error, while generalizing to the test set with an acceptable error, therefore, showing no signs of overfitting, despite the comparatively large size of the model. Finally, we would like to clarify that both the ANN and SVM results shown in Fig. 3 and 6 are the result of those 1000 reinitializations. Nonetheless, the random initializations of the ANN represent an additional source of variation to the cross-validation partitions, hence the comparison between both classifiers is not fair. It is to be noted that the ANN converged in approximately 4-5 different configurations, where most of the runs (~985/1000) presented a very closely related set of weights.

We agree with the authors that each criteria of principal component (PC) selection may provide a different number of PCs. It is to be noted that the results shown with 2 PCs (Fig. 5) were done to illustrate graphically the capabilities of discrimination using only two PCs. The results shown in Fig. 3 were obtained with all the PCs kept by Bartlett’s criterion. We acknowledge that by performing PCA out of the cross-validation loop, and retaining a portion of the 19 principal

# Antimycotic Activity Potentiation of *Allium sativum* Extract and Silver Nanoparticles against *Trichophyton rubrum*

Marissa Robles-Martínez,<sup>a</sup> Juan Fernando Cárdenas González,<sup>b</sup> Francisco Javier Pérez-Vázquez,<sup>c</sup> Juan Martín Montejano-Carrizales,<sup>d</sup> Elías Pérez,<sup>\*d</sup> and Rosalba Patiño-Herrera<sup>\*e</sup>

<sup>a</sup> Doctorado en Ingeniería y Ciencia de Materiales de la UASLP, Sierra Leona 530, San Luis Potosí, San Luis Potosí 78210, México

<sup>b</sup> Unidad Académica Multidisciplinaria Zona Media, UASLP, Rioverde, San Luis Potosí 79617, México

<sup>c</sup> Coordinación para la Innovación y Aplicación de la Ciencia y la Tecnología (CIACYT), UASLP, San Luis Potosí, San Luis Potosí 78210, México

<sup>d</sup> Instituto de Física, UASLP, Álvaro Obregón 64, San Luis Potosí 78000, México, e-mail: elias@ifiscia.uaslp.mx

<sup>e</sup> Departamento de Ingeniería Química, Tecnológico Nacional de México/Instituto Tecnológico de Celaya, Antonio García Cubas Pte #600 esq. Av. Tecnológico. Celaya, Guanajuato 38010, México, e-mail: roos\_ph@iqcelaya.itc.mx

A natural and biocompatible extract of garlic as a support, decorated with silver nanoparticles, is a proposal to generate an effective antifungal agent against dermatophytes at low concentrations. Silver nanoparticles (AgNPs) with a diameter of  $26 \pm 7$  nm were synthesized and their antimycotic activity was examined against *Trichophyton rubrum* (*T. rubrum*), inhibiting 94% of growth at a concentration of  $0.08 \text{ mg ml}^{-1}$ . *Allium sativum* (garlic) extract was also obtained (AsExt), and its MIC was  $0.04 \text{ mg ml}^{-1}$ . To increase the antifungal capacity of those systems, AsExt was decorated with AgNPs, obtaining AsExt-AgNPs. Using an AsExt concentration of  $0.04 \text{ mg ml}^{-1}$  in independent experiments with concentrations from 0.01 to  $0.08 \text{ mg ml}^{-1}$  of AgNPs, it was possible to inhibit *T. rubrum* at all AgNPs concentrations; it proves a synergistic effect between AgNPs and AsExt. Even if 1% of the minimum inhibitory concentration of AsExt ( $0.0004 \text{ mg ml}^{-1}$ ) is used, it was possible to inhibit *T. rubrum* at all concentrations of AgNPs, demonstrating the successful antimycotic activity potentiation when combining AsExt and AgNPs.

**Keywords:** antimycotic activity, potentiation, *Allium sativum* (garlic), silver nanoparticles, *Trichophyton rubrum*, biological activity.

## Introduction

Dermatophytes are common on tropical regions due to high humidity levels. During 2008, the rate of this fungal infection worldwide prevalence was of 20 to 25%,<sup>[1]</sup> hair keratin, skin and nails are its food source. The ability of dermatophytes to infect a host depends on several factors such as skin moisture, a slightly acidic pH, continuous skin regeneration, fatty acid conditions, keratinized state layer and the normal skin microbiota competition.<sup>[2]</sup> Infection begins with inoculation of spores deposited on a skin lesion or abrasion and its enzymatic ability to degrade keratin.<sup>[3]</sup> The

main dermatophytes that affect humans are *Epidermophyton*, *Microsporum* and *Trichophyton*.<sup>[4]</sup> Onychomycosis, also called tinea unguium or dermatophytic onychomycosis, is a fungal infection that damages the nail and skin nail union, and it affects about 10% of the adult population. This infection is caused mainly by *Trichophyton rubrum*, *Trichophyton mentagrophytes*, *T. interdigitale*, *Epidermophyton floccosum*, *T. violaceum*, *Microsporum gypseum*, *T. tonsurans* and *T. soudanense*.<sup>[5]</sup> Orally ingested medication that usually prescribed are griseofulvin, azole group different drugs (itraconazole, fluconazole, albaconazole, posaconazole, ravuconazole) and terbinafine. Nevertheless, there are



Article

# Altered erythrocyte morphology in Mexican adults with prediabetes and type 2 diabetes mellitus evaluated by scanning electron microscope

Alejandra Loyola-Leyva<sup>1</sup>, Juan Pablo Loyola-Rodríguez<sup>2,\*</sup>, Yolanda Terán Figueroa<sup>3</sup>, Francisco Javier González<sup>4</sup>, Marco Atzori<sup>5</sup>, and Simón Barquera Cervera<sup>6</sup>

<sup>1</sup>School of Medicine, Autonomous University of San Luis Potosí (Universidad Autónoma de San Luis Potosí), Avenida Venustiano Carranza 2405, Los Filtros, 78210, San Luis Potosí, S.L.P, Mexico, <sup>2</sup>Laboratory of Nanobiotechnology, Faculty of Medicine, Autonomous University of Guerrero (Universidad Autónoma de Guerrero), Acapulco, Guerrero, Mexico, <sup>3</sup>Faculty of Nursing and Nutrition, Autonomous University of San Luis Potosí (Universidad Autónoma de San Luis Potosí), Av. Niño Artillero 130. Zona Universitaria, 78240, San Luis Potosí, S.L.P, México, <sup>4</sup>Coordination for Innovation and Application of Science and Technology (CIACyT), Avenida Sierra Leona 550, Lomas 2<sup>a</sup> sección, 78210, San Luis Potosí, S.L.P, México, <sup>5</sup>Faculty of Sciences, Autonomous University of San Luis Potosí (Universidad Autónoma de San Luis Potosí), Lateral Av. Salvador Nava, Lomas, 78290, San Luis Potosí, S.L.P, México, and <sup>6</sup>National Institute of Public Health (Instituto Nacional de Salud Pública), Av. Universidad No.655 Col Sta. Ma. Ahuacatlán. Cuernavaca, Morelos, México

\*To whom correspondence should be addressed. E-mail: [juanpablo.loyola8@gmail.com](mailto:juanpablo.loyola8@gmail.com)

Received 28 October 2018; Editorial Decision 5 February 2019; Accepted 8 February 2019

## Abstract

**Aim:** To evaluate the erythrocyte morphology in people with prediabetes, T2DM and healthy subjects in a Mexican population and its association with biochemical parameters.

**Methods:** Cross-sectional study consisted of three groups: healthy (HG), people with prediabetes (PG) and with T2DM (DMG). A blood sample was obtained from all participants to assess the erythrocyte morphology, and levels of HbA1c, glucose and lipid profile. Anthropometrical parameters were also evaluated.

**Results:** It was observed that compared with healthy individuals, people with prediabetes presented a significant decrease in the diameter ( $-0.08\ \mu\text{m}$ ,  $P = 0.014$ ) and height ( $-0.07\ \mu\text{m}$ ,  $P = 0.004$ ), as well as people with T2DM ( $-0.33\ \mu\text{m}$ ,  $P < 0.001$  in diameter; and  $-0.36\ \mu\text{m}$ ,  $P < 0.001$  in height). Besides, it was found a significant difference in diameter ( $-0.25\ \mu\text{m}$ ,  $P < 0.001$ ) and height ( $-0.29\ \mu\text{m}$ ,  $P < 0.001$ ) between the PG and DMG. No significant differences in the axial ratio between groups. Also, HbA1c, glucose, triglycerides, cholesterol, LDL cholesterol, systolic blood pressure, weight, BMI, waist and hip circumference were significantly associated with diameter and height.



# A cost-effective method to prepare size-controlled nanoscale zero-valent iron for nitrate reduction

Claudio Adrian Ruiz-Torres<sup>1,2</sup>, René Fernando Araujo-Martínez<sup>1</sup>, Gabriel Alejandro Martínez-Castañón<sup>1</sup>, J. Elpidio Morales-Sánchez<sup>1</sup>, Tae-Jin Lee<sup>2</sup>, Hyun-Sang Shin<sup>2</sup>, Yuhoon Hwang<sup>2†</sup>, Abel Hurtado-Macías<sup>3</sup>, Facundo Ruiz<sup>1†</sup>

<sup>1</sup>Faculty of Sciences, The Autonomous University of San Luis Potosí (UASLP), Avenida Manuel Nava 6, Zona Universitaria, CP. 78290 San Luis Potosí, SLP., Mexico

<sup>2</sup>Department of Environmental Engineering, Seoul National University of Science and Technology, Seoul 01811, Republic of Korea

<sup>3</sup>Research Center for Advanced Materials (CIMAV), Ave. Miguel de Cervantes 120, Complejo Industrial Chihuahua, 31109 Chihuahua, Chihuahua, Mexico

## ABSTRACT

Nanoscale zero-valent iron (nZVI) has proved to be an effective tool in applied environmental nanotechnology, where the decreased particle diameter provides a drastic change in the properties and efficiency of nanomaterials used in water purification. However, the agglomeration and colloidal instability represent a problematic and a remarkable reduction in nZVI reactivity. In view of that, this study reports a simple and cost-effective new strategy for ultra-small (< 7.5%) distributed functionalized nZVI-EG (1-9 nm), with high colloidal stability and reduction capacity. These were obtained without inert conditions, using a simple, economical synthesis methodology employing two stabilization mechanisms based on the use of non-aqueous solvent (methanol) and ethylene glycol (EG) as a stabilizer. The information from UV-Vis absorption spectroscopy and Fourier transform infrared spectroscopy suggests iron ion coordination by interaction with methanol molecules. Subsequently, after nZVI formation, particle-surface modification occurs by the addition of the EG. Size distribution analysis shows an average diameter of 4.23 nm and the predominance (> 90%) of particles with sizes < 6.10 nm. Evaluation of the stability of functionalized nZVI by sedimentation test and a dynamic light-scattering technique, demonstrated very high colloidal stability. The ultra-small particles displayed a rapid and high nitrate removal capacity from water.

**Keywords:** Ethylene glycol, High colloidal stability, Nanoscale zero-valent iron (nZVI), Non-aqueous solvent, Stabilization mechanism, Ultra-small

## 1. Introduction

Alarming population growth and growing industrial activities, have led to elevated concentrations of a wide range of contaminants in wastewater and groundwater [1]. Nanoscale zero-valent iron (nZVI) has proved an effective tool for the treatment of wastewater because of their large surface area and specific affinity for toxic contaminants in aqueous systems [2]. However, the need to find materials with greater efficiency for this application persists. This improvement in efficiency is related to the dimensions and the uniformity of the diameters, and to the anti-aggregation capacity and colloidal stability, of the nanoparticles. In addition, they need

to be obtained using simple and economical synthesis methodologies to become a cost-effective solution in environmental remediation.

There are several reports of nanomaterials of zero-valent iron with ultra-small size and narrow size distribution (< 3-8 nm). These were made using synthetic techniques based on sonochemical decomposition of iron carbonyl, thermal decomposition of iron pentacarbonyl, and sonolysis of iron pentacarbonyl. The methodologies made use of a stabilizing agent of variable composition (polyvinylpyrrolidone (PVP), oleic acid (OA) oleylamine (OY), poly(ethyleneglycol) (PEG)), that intensified the reduction and control of particle size [3-6]. However, the synthesis techniques mentioned above are all extremely complex and expensive meth-



This is an Open Access article distributed under the terms of the Creative Commons Attribution Non-Commercial License (<http://creativecommons.org/licenses/by-nc/3.0/>) which permits unrestricted non-commercial use, distribution, and reproduction in any medium, provided the original work is properly cited.

Copyright © 2019 Korean Society of Environmental Engineers

Received September 6, 2018 Accepted November 2, 2018

† Corresponding author

Email: yhhwang@seoultech.ac.kr, facundo@ciencias.uaslp.mx

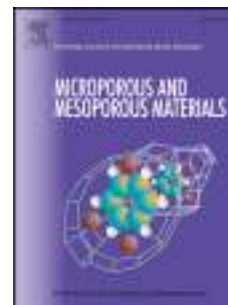
Tel: +82-2-970-6626, +52-444-826-2468 Fax: +82-2-971-5776, +52-444-826-2321

ORCID: 0000-0002-4013-3989 (Y. Hwang)

# Accepted Manuscript

H<sub>2</sub>Ti<sub>3</sub>O<sub>7</sub> titanate nanotubes for highly effective adsorption of basic fuchsin dye for water purification

Mariana Hinojosa-Reyes, Roberto Camposeco-Solis, Facundo Ruiz



PII: S1387-1811(18)30521-3

DOI: [10.1016/j.micromeso.2018.09.035](https://doi.org/10.1016/j.micromeso.2018.09.035)

Reference: MICMAT 9134

To appear in: *Microporous and Mesoporous Materials*

Received Date: 13 February 2018

Revised Date: 22 August 2018

Accepted Date: 28 September 2018

Please cite this article as: M. Hinojosa-Reyes, R. Camposeco-Solis, F. Ruiz, H<sub>2</sub>Ti<sub>3</sub>O<sub>7</sub> titanate nanotubes for highly effective adsorption of basic fuchsin dye for water purification, *Microporous and Mesoporous Materials* (2018), doi: <https://doi.org/10.1016/j.micromeso.2018.09.035>.

This is a PDF file of an unedited manuscript that has been accepted for publication. As a service to our customers we are providing this early version of the manuscript. The manuscript will undergo copyediting, typesetting, and review of the resulting proof before it is published in its final form. Please note that during the production process errors may be discovered which could affect the content, and all legal disclaimers that apply to the journal pertain.



Review

# Molecular Mechanisms of Bacterial Resistance to Metal and Metal Oxide Nanoparticles

Nereyda Niño-Martínez <sup>1</sup>, Marco Felipe Salas Orozco <sup>2,\*</sup> ,  
Gabriel-Alejandro Martínez-Castañón <sup>2</sup> , Fernando Torres Méndez <sup>2</sup> and Facundo Ruiz <sup>1</sup>

<sup>1</sup> Facultad de Ciencias, Universidad Autónoma de San Luis Potosí, San Luis Potosí Cp 78210, Mexico; nereyda.nino@uaslp.mx (N.N.-M.); ruizfacundo1@gmail.com (F.R.)

<sup>2</sup> Facultad de Estomatología, Universidad Autónoma de San Luis Potosí, San Luis Potosí Cp 78210, Mexico; mtzcastanon@ciencias.uaslp.mx (G.-A.M.-C.); fernando.torres@uaslp.mx (F.T.M.)

\* Correspondence: marco-salas@hotmail.com

Received: 12 May 2019; Accepted: 6 June 2019; Published: 8 June 2019



**Abstract:** The increase in bacterial resistance to one or several antibiotics has become a global health problem. Recently, nanomaterials have become a tool against multidrug-resistant bacteria. The metal and metal oxide nanoparticles are one of the most studied nanomaterials against multidrug-resistant bacteria. Several in vitro studies report that metal nanoparticles have antimicrobial properties against a broad spectrum of bacterial species. However, until recently, the bacterial resistance mechanisms to the bactericidal action of the nanoparticles had not been investigated. Some of the recently reported resistance mechanisms include electrostatic repulsion, ion efflux pumps, expression of extracellular matrices, and the adaptation of biofilms and mutations. The objective of this review is to summarize the recent findings regarding the mechanisms used by bacteria to counteract the antimicrobial effects of nanoparticles.

**Keywords:** bacteria; resistance; nanoparticles

## 1. Introduction

The increase in bacterial resistance to one or several antibiotics has become a global health problem [1]. The antibiotics were discovered in the 1920s. Since then, the discovery and use of new antibiotics have been accompanied by the appearance of bacterial resistance to them. The great genetic flexibility of the bacteria and the selection pressure exerted by the use of the antibiotics are responsible for the appearance and perpetuation of antibiotic resistance. Likewise, the variety of mechanisms of resistance to the different types of antibiotics has increased over time [2].

Recommendations have been suggested to avoid the constant appearance of resistance to antibiotics; these recommendations include: Improve sanitation and prevent the spread of infection, reduce unnecessary use of antimicrobials, improve global surveillance of drug resistance and antimicrobial consumption and promote rapid diagnostics techniques to reduce unnecessary use of antimicrobials. Likewise, new options for compounds with antimicrobial properties are continually being sought [3].

Recently, nanomaterials have become a tool against multidrug-resistant bacteria. These nanomaterials can be used as nano-drugs that can act individually or in synergism with antimicrobial compounds against resistant bacteria. Nanomaterials are also used as drug delivery systems that provide greater therapeutic efficacy and enhanced physicochemical characteristics. The metal and metal oxide nanoparticles are one of the most studied nanomaterials against multidrug-resistant bacteria. These nanoparticles can be synthesized from metals and metal oxides as gold, silver, titanium, copper, zinc, and aluminum; as well as silver oxide, copper oxide, magnesium oxide, calcium oxide, and zinc oxide.



## Revista Internacional de Investigación e Innovación Tecnológica

Página principal: [www.riit.com.mx](http://www.riit.com.mx)

---

### Permeability Fluid Test Prototype for Dental Sealers Using Digital Image Processing in LabVIEW

### Prototipo de Prueba de Permeabilidad de Fluidos para Selladores Dentales Utilizando Procesamiento Digital de Imágenes en LabVIEW

Martínez-Montejano, R.C.<sup>a\*</sup>, Netro-Grimaldo, J.F.<sup>a</sup>, Robles-Martínez, M.<sup>b</sup>, Jaime-Rodríguez, J.J.<sup>a</sup>, Gaitán-Fonseca, C.I.<sup>c</sup>, Aguilera-Galaviz, L.A.<sup>c</sup>, Pérez, E.<sup>d</sup>.

<sup>a</sup> Unidad Académica Multidisciplinaria Zona Media, Ingeniería Mecatrónica, Universidad Autónoma de San Luis Potosí, C. P. 79615. Rioverde, San Luis Potosí.

<sup>b</sup> Doctorado Institucional en Ciencia e Ingeniería de Materiales, Universidad Autónoma de San Luis Potosí, C. P. 78000, San Luis Potosí, San Luis Potosí.

<sup>c</sup> Unidad Académica de Odontología, Universidad Autónoma de Zacatecas, C. P. 98600, Guadalupe, Zacatecas.

<sup>d</sup> Instituto de Física, Universidad Autónoma de San Luis Potosí, C. P. 78000, San Luis Potosí, San Luis Potosí.

\*roberto.montejano@uaslp.mx

**Technological Innovation: Fluids permeability test instrumentation using digital pictures.  
Industrial Implementation Area: Odontology**

Received: June 12th, 2019

Accepted: October 20th, 2019

### Resumen

Un tratamiento endodóntico debe de ser capaz de prevenir el crecimiento bacteriano y la filtración de fluidos. Para poder probar la efectividad de un sellador dental, este debe de pasar por una serie de pruebas, dentro de las cuales se encuentra el método de penetración de fluidos. Esta prueba demuestra la capacidad de sellado de un cemento dental. El objetivo de este artículo consiste en presentar el trabajo de construcción de un prototipo para esta prueba que midiera cuantitativamente la microfiltración basada en la prueba de Pashley. El prototipo consiste de un tanque de oxígeno conectado a un sistema de presión que va hacia una caja acondicionada. Dentro de la caja, se encuentra una cámara USB con luz LED, una entrada de la caja, tiene adherida una jeringa y en la salida de la caja se ubica un diente obturado con el sellador. Se introduce una burbuja de aire en el sistema mediante la jeringa y la cámara USB monitorea el desplazamiento de la burbuja y el cálculo de la microfiltración es hecho mediante procesamiento digital de





## An algorithm for the *in situ* analysis of optical reflectance anisotropy spectra

J. Ortega-Gallegos<sup>a,\*</sup>, A. Lastras-Martínez<sup>a,\*</sup>, L.E. Guevara-Macías<sup>a</sup>, J.G. Santiago García<sup>a</sup>,  
D. Ariza-Flores<sup>a,b</sup>, R. Castro-García<sup>a,b</sup>, R.E. López-Estopier<sup>a,b</sup>, R.E. Balderas-Navarro<sup>a</sup>,  
L.F. Lastras-Martínez<sup>a</sup>



<sup>a</sup> Instituto de Investigación en Comunicación Óptica, Universidad Autónoma de San Luis Potosí, Alvaro Obregón 64, San Luis Potosí, SLP 78000, Mexico

<sup>b</sup> CONACyT - Instituto de Investigación en Comunicación Óptica, Universidad Autónoma de San Luis Potosí, Alvaro Obregón 64, San Luis Potosí, SLP 78000, Mexico

### ARTICLE INFO

Communicated by R.M. Biefeld

#### Keywords:

A1. Characterization  
A1. Growth models  
A1. Surface processes  
A3. Molecular beam epitaxy  
B2. Semiconducting gallium arsenide  
B2. Semiconducting III-V materials

### ABSTRACT

We report on a computer algorithm for the *in situ* analysis of reflectance anisotropy (RA) spectra in a time frame compatible with the epitaxial growth of cubic semiconductors. This algorithm allows for the *in situ* acquisition of RA spectra and their decomposition into two components whose amplitude depends on the As coverage of the semiconductor surface. One of such components is associated with the surface orthorhombic strain due to the surface reconstruction and has an amplitude that strongly depends with surface reconstruction and thus As coverage. This fact opens the possibility of using reflectance anisotropy spectroscopy (RAS) as an optical probe to characterize the As surface coverage in real time. To demonstrate the performance of the algorithm we report on RA measurements carried out during the homoepitaxial growth of GaAs (001). We show that the algorithm is capable of analyzing a set of 500 RA spectra in a time span of about 10 s. This allows for a range of applications for the developed algorithm, including the surface characterization and fine tuning of the substrate stoichiometry just before epitaxial growth, during the growth of the buffer layer.

### 1. Introduction

The growing complexity of advanced optoelectronic devices based on III-V semiconductors [1–3] demands probes for real-time growth monitoring with sub monolayer resolution. Non-invasive optical probes, such as reflectance anisotropy spectroscopy (RAS), are advantageous for this application given their high sensitivity, instrumental simplicity and fast response [4–6]. RAS is an optical polarization contrast technique, based on the measurements of difference of reflectivity for two orthogonal polarized light beams [8]. This spectroscopy enhances the surface related response by taking advantage of the reduced symmetry of the surface region of a cubic crystal. We note that for polarizations of the incident beam parallel to the principal axes of the crystal, the signal arising from the isotropic bulk is suppressed [4,5,9,10].

The usefulness of RAS as a surface characterization technique stems from the strong dependence of the reflectance anisotropy (RA) line shape on surface reconstruction [4–7]. In this respect, GaAs surfaces with reconstructions  $c(4 \times 4)$  and  $(2 \times 4)$  show characteristic and well differentiated RA lineshapes. However, despite the fact that the surface specificity of anisotropic reflectance has been recognized for a long time [11], the development of the full potential of the technique for the

real-time characterization of epitaxial growth has been traditionally hampered by the lack of anisotropic reflectance spectrometers with high enough, both, spectrum acquisition speed and spectral resolution.

Recently, we developed a rapid RA 32-channel spectrometer with the capability to measure in real-time fractional changes of monolayer coverage during epitaxial growth [12]. Taking advantage of such instrument, we carried out a series of real-time RAS measurements during the homoepitaxial growth of GaAs (001) under several  $As_4$  overpressures and found that upon starting growth on an As-rich surface ( $c(4 \times 4)$  reconstruction), the RAS amplitude undergoes a fast transient towards a less As-rich surface ( $(2 \times 4)$  reconstruction). This transient is a function of both As overpressure and substrate temperature and takes place within the first monolayer (ML) growth period.

RA line shapes are, nevertheless, complex and not readily interpreted. Indeed, previously we have shown that the reflectance anisotropy (RA) spectra of both  $c(4 \times 4)$  and  $(2 \times 4)$  surfaces comprise two spectral components whose relative amplitude is a function of surface As coverage [13]. A first component is associated with the orthorhombic strain induced by surface reconstruction and its amplitude changes sign when shifting from  $c(4 \times 4)$  to  $(2 \times 4)$  reconstruction [13]. A second component shows an amplitude variation with no change of sign [16]. Additionally, it is noted that the RAS oscillations are mainly

\* Corresponding authors.

E-mail addresses: [jortega@cactus.iico.uaslp.mx](mailto:jortega@cactus.iico.uaslp.mx) (J. Ortega-Gallegos), [alm@cactus.iico.uaslp.mx](mailto:alm@cactus.iico.uaslp.mx) (A. Lastras-Martínez).

<https://doi.org/10.1016/j.jcrysgr.2019.03.002>

Received 15 November 2018; Received in revised form 5 February 2019; Accepted 1 March 2019

Available online 02 March 2019

0022-0248/ © 2019 Elsevier B.V. All rights reserved.



# Extender sets and measures of maximal entropy for subshifts

Felipe García-Ramos and Ronnie Pavlov

## ABSTRACT

For countable amenable finitely generated torsion-free  $\mathbb{G}$ , we prove inequalities relating  $\mu(v)$  and  $\mu(w)$  for any measure of maximal entropy  $\mu$  on a  $G$ -subshift and any words  $v, w$  where the extender set of  $v$  is contained in the extender set of  $w$ . Our main results are two generalizations of a theorem of Meyerovitch (*Ergodic Theory Dynam. Systems* 33 (2013) 934–953): the first applies to all such  $v, w$  when  $\mathbb{G} = \mathbb{Z}$ , and the second to  $v, w$  with the same shape for any  $\mathbb{G}$ . As a consequence of our results we give new and simpler proofs of several facts about synchronized subshifts (including a result from Thomsen, *Ergodic Theory Dynam. Systems* 26 (2006) 1235–1256) and we answer a question of Climenhaga.

## 1. Introduction

In this paper, we prove several results about measures of maximal entropy on symbolic dynamical systems (subshifts). Measures of maximal entropy are natural measures, defined via the classical Kolmogorov–Sinai entropy, which also connect to problems in statistical physics, such as existence of phase transitions.

Our dynamical systems are subshifts, which consist of a compact  $X \subseteq \mathcal{A}^{\mathbb{G}}$  (for some finite alphabet  $\mathcal{A}$  and a countable amenable finitely generated torsion-free group  $\mathbb{G}$ ) and dynamics given by the  $\mathbb{G}$ -action of translation/shift maps  $\{\sigma_g\}_{g \in \mathbb{G}}$  (under which  $X$  must be invariant). Subshifts are useful both as discrete models for the behavior of dynamical systems on more general spaces, and as an interesting class of dynamical systems in their own right, with applications in physics and information theory.

Our main results show that when a word  $v$  (that is, an element of  $\mathcal{A}^F$  for some finite  $F \subset \mathbb{G}$ ) is replaceable by another word  $w$  in  $X$  (meaning that  $\forall x \in X$ , when any occurrence of  $v$  is replaced by  $w$ , the resulting point is still in  $X$ ), there is a simple inequality relating  $\mu(v)$  and  $\mu(w)$  for every measure of maximal entropy (MME)  $\mu$ . (As usual, the measure of a finite word is understood to mean the measure of its cylinder set; see Section 2 for details.) A formal statement of our hypothesis uses extender sets [7, 19]; the condition ‘ $v$  is replaceable by  $w$ ’ is equivalent to the containment  $E_X(v) \subseteq E_X(w)$ , where  $E_X(u)$  denotes the extender set of a word  $u$ .

For  $\mathbb{Z}$ -subshifts specifically, it is possible to talk about replacing  $v$  by  $w$  (and thereby the containment  $E_X(v) \subseteq E_X(w)$ ) even if their lengths  $|v|$  and  $|w|$  are different, and our first results treat this case.

**THEOREM 3.11.** *Let  $X$  be a  $\mathbb{Z}$ -subshift with positive topological entropy,  $\mu$  an MME of  $X$ , and  $w, v \in L(X)$ . If  $E_X(v) \subseteq E_X(w)$ , then*

$$\mu(v) \leq \mu(w)e^{h_{\text{top}}(X)(|w|-|v|)}.$$

---

Received 29 October 2018; revised 19 May 2019; published online 25 June 2019.

2010 *Mathematics Subject Classification* 37B10, 37B40, 37A35 (primary), 37A60 (secondary).

The second author gratefully acknowledges the support of NSF grant DMS-1500685.

# Performance improvement of refractometric sensors through hybrid plasmonic-Fano resonances

Mahmoud H. Elshorbagy, Alexander Cuadrado, Gabriel González,  
Francisco J. González *Senior Member, IEEE*, and Javier Alda *Member, OSA*

**Abstract**—In this paper, we present a plasmonic refractometric sensor that works under normal incidence; allowing its integration on a fiber tip. The sensor's material and geometry exploit the large scattering cross-section given by high-contrast of the index of refraction subwavelength dielectric gratings. Our design generates a hybrid plasmonic-Fano resonance due to the interference between the surface plasmon resonance and the grating response. We optimize the sensor with a merit function that combines the quality parameter of the resonance and the field enhancement at the interaction volume where the plasmon propagates. Our device shows a high sensitivity (1000 nm/RIU) and a high Figure of Merit ( $775 \text{ RIU}^{-1}$ ). Degradation in performance is negligible through a wide dynamic range up to 0.7 RIU. These quantitative parameters overperform compared to similar plasmonic sensors.

**Index Terms**—plasmonics, optical sensors, Fano resonances.

## I. INTRODUCTION

Photonic nanostructures control light propagation through optical media. They can function as perfect absorbers [1], [2], efficient scatterers [3], [4], frequency selective surfaces [5]–[7], etc. Optical sensors based on surface plasmon resonances (SPR) benefit from the use of nanostructures for an increased range of applications with improved performance. For example, they are applied to colorimetry [8], and refractometers for gases [9], bio-fluids [10], and chemicals [11]. A change in refractive index of the media can be measured with a conventional plasmonic device in Kretschmann configuration, where the reflectance dip is located and measured angularly [12]. In this setup, the key aspects for device performance are: the material and thickness of the metal layer, the refractive index of the prism, the angle of incidence, and the wavelength of the resonance. For angular interrogation, the maximum theoretical value of sensitivity of a Kretschmann configuration based sensor is  $600 \text{ deg/RIU}$  [12]. This extreme value is achieved with a low index prism ( $n = 1.32$ ) and an angle of incidence of  $\sim 81^\circ$ . The need of a low index of refraction is strongly limited by material availability. Some polymers, such as Cytop<sup>TM</sup>, reach very low values of the index of refraction ( $n_{\text{Cytop}} = 1.34$ ) [13]. Here, we select magnesium fluoride,  $\text{MgF}_2$  ( $n_{\text{MgF}_2} = 1.37$ ), because it is

commercially available, transparent within the spectral region of interest ( $\lambda \in [1300, 2000] \text{ nm}$ ), and has a very low index of refraction. Moreover,  $\text{MgF}_2$  produces planar interfaces when coating nanostructured reliefs [14]. The angle of incidence and material constrains of Kretschmann configuration lead to a narrow dynamic detection range [12]. To overcome this limit, the community has proposed different configurations of SPR sensors; including spectral interrogation and more sophisticated geometries [15]–[19].

The performance parameters of a SPR sensor are: sensitivity, Figure of Merit (FOM), resolution, linearity, dynamic range, and reproducibility [20]. Sensitivity is the shift of a measurable parameter of the device (a dip in reflectance, transmission, absorption, phase, temperature, etc.) respect to a controlled variable (angle, wavelength, power, etc.) due to a change in the sensed property (refractive index, specimen concentration, color, etc.) [20]. FOM combines sensitivity and the spectral line-shape characteristics in a parameter that compares sensors, independent from the interrogation strategy (angular, spectral, etc.). Resolution is the minimum change of the sensed property measured by the device. Linearity is assured if sensitivity is constant through the entire dynamic range of the sensor. Although high linearity response devices have been reported, the measured shift is not fully linear [16]. The dynamic range is the interval of the sensed property where the sensor works optimally. In refractometric sensors, recent contributions show high efficiency devices with wide dynamic range up to 0.5 RIU [15]–[19], including devices with adjustable dynamic range [21]. In summary, it is very challenging to design an efficient sensor with high sensitivity, large FOM, good resolution, linearity, wide dynamic range, reliability and reproducibility.

Many approaches enhance performance of SPR optical sensors with bi-metals [22], buffer layers [23], and nanoparticles [24]. The integration of plasmonic sensors with optical fibers and waveguides leads to high performance systems [25] that work in both liquids and gases [26]. Moreover, other groups show integrated devices that excite surface plasmon resonances at normal incidence [27]–[32]. These proposals integrate the sensor at the end of optical fibers or wave-guides. Furthermore, the key elements for competitive and practical devices are: feasible and fabricable geometries and features, compatible material combinations for various applications, and high performance.

The operation of a spectrally-interrogated plasmonic sensor relies on the precise measurement of the spectral location of the minimum (or maximum) of its response. A narrow

M. H. Elshorbagy, A. Cuadrado, and J. Alda are with Applied Optics Complutense Group. University Complutense of Madrid. Faculty of Optics and Optometry. Av. Arcos de Jalon, 118. 28037 Madrid, Spain.

M. H. Elshorbagy is also with Physics Department. Faculty of Science. Minia University. 61519 El-Minya, Egypt.

G. González, and F. J. González are with Universidad Autónoma de San Luis Potosí. Av. Sierra Leona, 550, Col. Lomas 2a. Sección. 78210 San Luis Potosí, México.

Corresponding author: Javier Alda, javier.alda@ucm.es

**RESEARCH ARTICLE**

# Characterization of wild-type and mutant p53 protein by Raman spectroscopy and multivariate methods

Karen Hernández-Vidales<sup>1</sup> | Edgar Guevara<sup>1,2</sup> | Vanesa Olivares-Illana<sup>3</sup> | Francisco Javier González<sup>1</sup> <sup>1</sup>Terahertz Science and Technology Center (C2T2) and Terahertz Science and Technology National Laboratory

(LANCYTT), Universidad Autónoma de San Luis Potosí, San Luis Potosí, México

<sup>2</sup>CONACYT-Universidad Autónoma de San Luis Potosí, San Luis Potosí, México<sup>3</sup>Laboratorio de Interacciones Biomoleculares y Cancer, Instituto de Física, Universidad Autónoma de San Luis Potosí, San Luis Potosí, México**Correspondence**

Edgar Guevara, CONACYT-Universidad Autónoma de San Luis Potosí, San Luis Potosí, México.

Email: eguevara@conacyt.mx

**Funding information**

Consejo Nacional de Ciencia y Tecnología, Grant/Award Numbers: Cátedras CONACYT program project 528, National Labs program through LANCYTT, the Teraher PhD scholarship No. 293704 Project 105 of “Centro Mexicano de Innovación e, 293704 and 528; Terahertz Science and Technology National Laboratory; Centro Mexicano de Innovación en Energía Solar, Grant/Award Number: 105

**Abstract**

To improve the early and reliable detection of cancer novel methods for the identification of associated biomarkers can suppose a big advantage over most of the techniques nowadays used for diagnosis because these techniques generally have the disadvantages of being laborious, invasive, and dependent on the physician's experience. The cancer biomarker wild-type p53 protein is naturally present in the human body and activated when cellular damage is detected. Mutations in p53 are related to the presence of tumors.

In this work, Raman spectra of wild-type and mutant p53 were obtained. The spectra were analyzed by multivariate methods. Principal component analysis and support vector machine algorithms showed that it is possible to discriminate between the wild and mutant types of this biomarker with an accuracy of 94%. An estimation of the limit of the detection of the wild-type p53 protein by means of Raman spectroscopy was performed by partial least squares regression, reaching that it is possible to detect concentration as low as 0.946  $\mu\text{M}$  without additional reagents. This proof-of-concept test shows that it is possible to detect and differentiate among types of p53 and represent the basis for an advanced study where a mechanism of signal amplification can be implemented. Raman spectroscopy in conjunction with multivariate mathematical techniques is projected as a complete tool capable of identifying biomarkers in a noninvasive, simple, and economical way, eliminating the subjective interpretation of the results, and therefore contributing to objective and more reliable diagnoses.

**KEYWORDS**

multivariate methods, p53 protein, Raman spectroscopy

## 1 | INTRODUCTION

The timely and reliable detection of mortal sickness such as cancer is most of the time a deciding factor between life and death of the patient.<sup>[1–3]</sup> Unfortunately, detecting cancer in early stages is complicated because generally, there are no symptoms of the disease and most of the

common techniques employed to screen certain types of cancer are based on clinical examination whose results depend largely on the physician expertise. To conclude with a definitive diagnosis, several studies are implemented to find an indicator that confirms or discards the presence of malignant tissue: laboratory tests, imaging studies, and biopsy; however, interpretation of the



# Analysis of vibrational modes from alpha-synuclein: a theoretical model using density functional theory and Raman spectroscopy

Fabiola León-Bejarano<sup>1</sup> · Miguel G. Ramírez-Elías<sup>1</sup> · Martín O. Méndez<sup>2</sup> · Ricardo A. Guirado-López<sup>3</sup> · Alfonso Alba<sup>2</sup> · Ildelfonso Rodríguez-Leyva<sup>4</sup>

Received: 15 January 2019 / Accepted: 22 August 2019 / Published online: 13 September 2019  
© IUPESM and Springer-Verlag GmbH Germany, part of Springer Nature 2019

## Abstract

Parkinson's disease is a neurodegenerative pathology difficult to diagnose. Researches have confirmed the presences of death cells in the brain produced by the modification of a protein called alpha-synuclein synuclein in people with Parkinson disease. Currently, a great amount of research is conducted to identify its biomarkers for early diagnostics. Recently, a studio found differences between the alpha- synuclein of the skin from Parkinson's disease and normal patients. In this paper, we use Raman spectroscopy through a numerical model to simulate the vibrational modes of well-defined finite clusters of alpha-synuclein in normal and pathological state, using the Gaussian09 software. The results of the model in the range of  $x - y \text{ cm}^{-1}$  are in good agreement with the experimental Raman spectra acquired from human skin with alpha-synuclein in the normal and pathological state.

**Keywords** Raman spectroscopy · Parkinson's disease · Density Functional theory · Alpha-synuclein

## 1 Introduction

Neurodegenerative diseases (ND) imply progressive degeneration of neurons in some areas of the brain. Studies suggest that this degeneration is due to the conformational change of a protein called alpha-synuclein that cause toxicity, and finally induces degradation in functions generally associated with the nervous system [1, 2]. The older population (>60 years old) is affected by this kind of pathologies. According to the prevalence of these disorders, currently, these are considered a public health problem due to the rising life expectancy of the people. Parkinson's disease (PD) is one of the most prevalent NDs. It is diagnosed using clinical criteria, such as symptomatology, laboratory studies to detect smells, video fluorography, and neuroimaging studies. PD

is characterized by the presence of tremor, rigidity, akinesia, bradykinesia, postural alteration, unilateral dystonia, ideomotor apraxia, dysphagia, personality changes, dementia, depression, and a decrease of olfaction. However, there is little knowledge of PD, and its biomarkers are still being determined. Consequently, PD is usually diagnosed once the symptoms are evident; that is, at its advanced stages [3–6]. Recent research has studied methods detecting of non-invasive biological markers for early and prompt diagnosis, and it has found that people with PD show aggregates of the alpha-synuclein protein in the brain. Such results suggest that these aggregates (overexpression) are responsible for cell death and have an important role in the neurodegeneration [7].

Alpha-synuclein is the largest fibril constituent from Lewy bodies in dopaminergic neurons in the substantia nigra, which are the main characteristic of the PD.

Recent research, based on biopsies of skin from people with PD has demonstrated differences in the alpha-synuclein morphology between skin from PD patients and healthy people (associated with the aggregates of alpha-synuclein in the brain) [8]. Thus, this study suggests the analysis of the conformational state of alpha-synuclein for diagnostic purposes. However, the use of skin biopsies is an invasive procedure that should be done by qualified personnel. As a consequence, this entails to the search of methods to quantify the difference between the healthy skin and PD, in an easy, quickly and noninvasive way.

✉ Fabiola León-Bejarano  
fabiolamlb@gmail.com

<sup>1</sup> Facultad de Ciencias, Universidad Autónoma de San Luis Potosí, San Luis Potosí, S. LP, Mexico

<sup>2</sup> Laboratorio Nacional CI3M & CICSaB, Universidad Autónoma de San Luis Potosí, San Luis Potosí, S. LP, Mexico

<sup>3</sup> Instituto de Física, Universidad Autónoma de San Luis Potosí, San Luis Potosí, S. LP, Mexico

<sup>4</sup> Facultad de Medicina, Universidad Autónoma de San Luis Potosí, San Luis Potosí, S. LP, Mexico

# Prediction of epileptic seizures using fNIRS and machine learning

Edgar Guevara<sup>a,f</sup>, Jorge-Arturo Flores-Castro<sup>b</sup>, Ke Peng<sup>c</sup>, Dang Khoa Nguyen<sup>d</sup>, Frédéric Lesage<sup>c,e</sup>, Philippe Pouliot<sup>c,e</sup> and Roberto Rosas-Romero<sup>b,\*</sup>

<sup>a</sup>CONACYT - Universidad Autónoma de San Luis Potosí, Sierra Leona, Lomas 2a. secc., San Luis Potosí, Mexico

<sup>b</sup>Universidad de las Américas - Puebla, Sta. Catarina Mártir. Cholula, Puebla. C.P. 72820, Mexico

<sup>c</sup>École Polytechnique de Montréal, Department of Electrical Engineering, C.P. 6079 succ. Centre-ville, Montréal, Québec H3C 3A7, Canada

<sup>d</sup>Hôpital Notre-Dame du CHUM, Neurology Division, 1560 rue Sherbrooke est, Montréal, Québec H2L 4M1, Canada

<sup>e</sup>Montreal Heart Institute, 5000 Bélanger Street, Montréal, Québec HIT 1C8, Canada

<sup>f</sup>Terahertz Science and Technology Center (C2T2) and Science and Technology National Lab (LANCyTT), Universidad Autónoma de San Luis Potosí, Mexico

**Abstract.** Research to predict epileptic seizures has been mainly focused on the analysis of *electroencephalography* (EEG) signals; however, recent research efforts have encouraged the use of a relatively new optical signal modality, called *functional Near-Infrared Spectroscopy* (fNIRS). In fNIRS, near-infrared light is injected into the scalp and the intensity of the reflected light is registered in optodes. Light absorption in hemoglobin depends on the level of blood oxygenation, which is related to brain activity. In this technique, two parameters are measured at each optode, the relative level of *oxygenated hemoglobin* (HbO) and the relative level of *deoxygenated hemoglobin* (HbR).

In this work we investigated the feasibility of predicting epileptic seizures, using either fNIRS, EEG, or a combination of both signals. In one set of experiments, different implementations for epileptic seizure prediction are tested by using (1) different combinations of electrical and optical signals (EEG, HbO, HbR, EEG+HbO, EEG+HbR, HbO+HbR, EEG+HbO+HbR) and (2) two different classifiers, (*Support Vector Machine* - SVM and *Multi-Layer Perceptron* - MLP). In the second set of experiments, seizures are predicted within a five-minute window that is moved up to 15 minutes before the start of the epileptic seizure.

By computing the *Positive Predictive Value* (PPV) and the *accuracy*, it is demonstrated that fNIRS-based epileptic prediction outperforms EEG-based epileptic prediction. By using optical signals and the SVM classifier, a PPV greater than 99% and an *accuracy* of 100% were obtained. PPV values of 100% are also obtained when seizures are predicted up to 15 minutes in advance. Furthermore, *Kernel Discriminant Analysis* (KDA) is used to demonstrate that the highest separability among the classes, corresponding to different epileptic signal phases (*pre-ictal*, *ictal*, and *inter-ictal*), is achieved when fNIRS recordings are used as features for prediction. Finally, fNIRS-based epileptic seizure prediction is tested with *Random Chance* classifiers.

In this study, we showed that fNIRS signals are an effective tool to predict epileptic seizures, even without the use of EEG signals, which are the current standard for seizure prediction.

**Keywords:** epileptic seizure, seizure prediction, functional near infra red spectroscopy (fNIRS), electroencephalogram (EEG), multi-layer perceptron (MLP), support vector machine (SVM)

\*Corresponding author. Roberto Rosas-Romero, Universidad de las Américas - Puebla, Sta. Catarina Mártir. Cholula, Puebla. C.P. 72820, Mexico. E-mail: roberto.rosas@udlap.mx.

## Low-cost embedded system for optical imaging of intrinsic signals

E. Guevara<sup>a,b,\*</sup>, M. Miranda-Morales<sup>c</sup>, K. Hernández-Vidales<sup>b</sup>, M. Atzori<sup>c</sup>, and F.J. González<sup>b</sup>

<sup>a</sup>CONACyT-Universidad Autónoma de San Luis Potosí, Mexico.

<sup>\*</sup>e-mail: edgar.guevara@uaslp.mx

<sup>b</sup>Terahertz Science and Technology Center (C2T2) and Science and Technology National Lab, Universidad Autónoma de San Luis Potosí, Sierra Leona 550 Lomas 2a secc. San Luis Potosí, SLP, 78210 Mexico.

<sup>c</sup>Neurobiology of Stress Laboratory, Facultad de Ciencias, Universidad Autónoma de San Luis Potosí, Mexico.

Received 2 May 2019; accepted 26 June 2019

This paper describes the proof-of-concept evaluation of a low-cost imaging system for obtaining functional connectivity maps of *in vivo* murine models. This non-contact system is based on the Raspberry Pi 3 and its V2 camera and offers a method for obtaining resting-state images of brain activity without the use of extrinsic contrast agents. The system was fully characterized in terms of dark signal, linearity, sensor noise resolution, and spatial frequency response. One mouse was observed *in vivo*, and functional connectivity maps were obtained by combining resting-state analysis and optical intrinsic signals imaging. Intra-mouse variations in functional connectivity remain consistent across multiple imaging sessions. In principle, inexpensive optical imaging of intrinsic signals allows the study of the mechanisms underlying human brain disorders in well-controlled murine models.

**Keywords:** Optical instruments and equipment; neuroscience; image forming and processing; data acquisition; hardware and software.

PACS: 07.60.j; 87.19.La; 42.30.Va; 07.05.Hd.

DOI: <https://doi.org/10.31349/RevMexFis.65.651>

### 1. Introduction

Optical imaging of intrinsic signals (OIS) is a technique that employs a digital camera to record images of the brain, while specific wavelengths of light are shunned upon the cortical surface. Relative changes in reflected light intensity correspond to relative changes in the local concentrations of oxygenated hemoglobin and deoxygenated hemoglobin. OIS series of images represent a bidimensional functional map of hemodynamic signals, which are a proxy of neural activity [1]. Briefly, when a neuron fires, there is a localized consumption of oxygen revealed by an initial augmentation in deoxygenated hemoglobin. One or two seconds later, there is a large increase in cerebral blood flow and cerebral blood volume as a compensatory process to the initial oxygen consumption. This large discrepancy between oxygen utilization and supply prompts a delayed increase in the local concentration of oxygenated hemoglobin and the ensuing dilution of deoxygenated hemoglobin. Therefore, neural activity can be indirectly quantified and localized by measuring hemodynamic changes [2]. In small mammal models, OIS is usually performed through the intact skull of the animal, with the scalp carefully removed, as in this work. Certainly, with larger animals, OIS needs to carry out OIS through the thinned skull with a rotative tool [3]. Can be extended to study optogenetically evoked signals, although it requires transgenic mice expressing channelrhodopsin (ChR2) [4], it can be performed in isolated brain slices *ex vivo* [1] or facilitated through the use of an intracranial transparent window [5]. OIS has been employed as a diagnostic tool, taking advantage of the intrinsic contrast provided by hemoglobin,

which allows imaging without the addition of external contrast reagents. Its numerous theoretical and empirical advantages position this modality as a strong candidate to study the brain in murine models of neurological conditions [6]. Two of the greatest advantages over other brain imaging modalities are the use of non-ionizing radiation and its moderate cost [5]. Conventional techniques used to acquire OIS images rely on scientific-grade charged-couple device (CCD) or complementary metal-oxide-semiconductor (CMOS) of the so-called scientific-grade, which cost between \$2600 USD (PhotonFocus MV1-D1024E-160-CL-12) to \$9000 USD (Teledyne DALSA Pantera 1M30), plus the added cost of a macro lens and a computer with a frame grabber. The use of a Raspberry Pi with its CMOS V2 camera module [7] retains the advantage of using nonionizing radiation and further reduces the cost by approximately 1.5 orders of magnitude. Hence, our motivation to explore this technique in a low-cost platform, which would empower the scientific community with a portable, inexpensive instrument to map the brain of small animal models. Functional imaging has been previously performed with a Raspberry and its camera [8], however extrinsic contrast, in the form of genetically modified mice expressing light-sensitive protein was employed. The use of wild-type mice provides a quick, simple, and inexpensive way to study brain function in a non-contact fashion with Raspberry-based OIS apparatus. The main goal of this work is to characterize the capabilities of this imaging setup free of extrinsic contrast and provide a proof of concept application in a mouse.



## Effects of Mg incorporation in cubic GaN films grown by PAMBE near Ga rich conditions



V.D. Compeán-García<sup>a</sup>, H. Moreno-García<sup>b</sup>, E. López-Luna<sup>b</sup>, H. Pérez Ladrón de Guevara<sup>c</sup>,  
A. Escobosa Echavarría<sup>d</sup>, Y. Kudriavtsev<sup>d</sup>, F.J. Rodríguez-Aranda<sup>b</sup>, A.G. Rodríguez<sup>b</sup>, M.A. Vidal<sup>b,\*</sup>

<sup>a</sup> CONACyT-Coordinación para la Innovación y Aplicación de la Ciencia y Tecnología (CIACyT), Universidad Autónoma de San Luis Potosí (UASLP), Álvaro Obregón 64, San Luis Potosí 78000, Mexico

<sup>b</sup> Coordinación para la Innovación y Aplicación de la Ciencia y Tecnología (CIACyT), Universidad Autónoma de San Luis Potosí (UASLP), Álvaro Obregón 64, San Luis Potosí 78000, Mexico

<sup>c</sup> Centro Universitario de los Lagos, Universidad de Guadalajara, Av. Enrique Díaz de León 1144, col. Paseos de la Montaña, Lagos de Moreno, Jalisco 47460, Mexico

<sup>d</sup> Electric Engineering Department, Centro de Investigación y Estudios Avanzados del IPN, Apartado Postal 14-740, 07000 México D.F., Mexico

### ARTICLE INFO

#### Keywords:

Cubic GaN diode  
Mg p-type doping  
Plasma-assisted molecular beam epitaxy

### ABSTRACT

The structural and electrical properties of Mg-doped cubic GaN epi-layers grown by plasma-assisted molecular beam epitaxy (PAMBE) near Ga rich conditions are investigated. The diffraction of high-energy reflected electrons (RHEED) in situ, in addition to structural studies of X-ray diffraction, show that the fraction of hexagonal and crystal twinning inclusions decreases when the Mg flux increases. The condition for the higher incorporation of Mg where the electrical properties are optimized is highly sensitive to the flow ratio Mg/Ga. The p-doping level steadily increases with increasing Mg flux. The Mg concentration obtained by secondary ion mass spectroscopy (SIMS) from samples grown at Mg temperatures from 200 °C to 700 °C are in a range between  $2 \times 10^{19}$  to  $2 \times 10^{20}$  atoms/cm<sup>3</sup>. The highest mobility and p-type doping level achieved, determined from Hall measurements, were 28.2 cm<sup>2</sup>/V-s and  $2 \times 10^{19}$  cm<sup>-3</sup>, respectively. We corroborate that the Mg doped c-GaN films are suitable for the construction of optoelectronic devices based on cubic III-Nitrides.

### 1. Introduction

Cubic gallium nitride (c-GaN) has a bandgap of 200 meV lower than the hexagonal phase (h-GaN) [1], for this reason, it is possible to modulate to the visible region with less amount of indium in the zinc-blend than wurtzite InGaN alloy [2–5]. In addition, due to higher crystalline symmetry, resulting in more isotropic properties and no spontaneous polarization induced-electric fields in the direction parallel to the c-axis, it is possible to grow the cubic InGaN alloy with a bandgap in the green region [2–9]. Consequently, this alloy is attractive for applications in photovoltaic and optoelectronic devices, including multiband solar cells, hydrogen production photoelectrodes, laser and light emitting diodes [10].

However, the development of optoelectronic, photovoltaic and electronic devices based on c-InGaN requires an efficient p-type doping and high-quality crystal structure. To our knowledge, limited reports of cubic III-Nitrides devices have been found in the literature [11,12], this is in part for the inefficient p-type doping or the main disadvantage in the synthesis of c-GaN, the lack of native substrates and a low-quality

crystalline film due to the hexagonal inclusions [13,14]. Therefore, improvements in the efficiency of p-type doping of the c-GaN epilayers are essential for enhanced manufacturing technology of cubic III-Nitrides semiconductors.

This paper presents a study of the influence of the Mg flux on the electrical and structural properties of Mg doping c-GaN, grown by molecular beam epitaxy on MgO (100) substrates, near to the regimen of Ga rich conditions. This study is performed by varying the Mg flux (with magnesium effusion cell temperature in a range from 200 to 700 °C) with growth conditions of c-GaN films at 720 °C.

### 2. Experimental

Epitaxial growth of Mg-doped c-GaN films heterostructures under study was performed on 1 cm<sup>2</sup> MgO(001) substrates by a vertical PAMBE with standard effusion cells for Ga, Mg, and an high-purity N<sub>2</sub> RF plasma cell [2,6]. The purity of Ga and Mg sources are 99.9995%.

Prior to the growth of the Mg-doped GaN epi-layer, the substrate was cleaned on a 10 min trichloroethylene and acetone ultrasonic bath.

\* Corresponding author.

E-mail address: [miguel.vidal@uaslp.mx](mailto:miguel.vidal@uaslp.mx) (M.A. Vidal).

<https://doi.org/10.1016/j.mssp.2018.12.019>

Received 8 November 2018; Received in revised form 17 December 2018; Accepted 19 December 2018

Available online 11 January 2019

1369-8001/ © 2018 Published by Elsevier Ltd.



**High-pressure structural change in the ferroelectric layered perovskite  $\text{Sr}_2\text{Nb}_2\text{O}_7$** 

Javier Alanis,<sup>1</sup> Hiram Joazet Ojeda-Galván,<sup>1,2</sup> M. C. Rodríguez-Aranda,<sup>2,\*</sup> A. G. Rodríguez,<sup>2</sup> Harumi Moreno García,<sup>2</sup> Jorge Íñiguez,<sup>3,4</sup> María Eugenia Mendoza,<sup>1</sup> and Hugo R. Navarro-Contreras<sup>2,\*</sup>

<sup>1</sup>*Instituto de Física, Benemérita Universidad Autónoma de Puebla, Av. San Claudio and Boulevard 18 Sur,*

*Col. San Manuel, Ciudad Universitaria, Puebla, Pue. 72570, México*

<sup>2</sup>*Coordinación para la Innovación y Aplicación de la Ciencia y la Tecnología (CIACYT),*

*Universidad Autónoma de San Luis Potosí, Álvaro Obregón 64, San Luis Potosí, S.L.P. 78000, México*

<sup>3</sup>*Materials Research and Technology Department, Luxembourg Institute of Science and Technology (LIST),*

*Maison de l'innovation 5, Avenue des Hauts-Fourneaux, L-4362 Esch-sur-Alzette, Luxembourg*

<sup>4</sup>*Physics and Materials Research Unit, University of Luxembourg, 41 Rue du Brill, L-4422 Belvaux, Luxembourg*



(Received 28 March 2019; revised manuscript received 26 June 2019; published 26 August 2019)

The structural changes of sintered powder samples of perovskite-slab layered polycrystalline  $\text{Sr}_2\text{Nb}_2\text{O}_7$  (SNO) ferroelectric compound subjected to high pressures are here investigated. The samples were prepared using a solid-state reaction in the presence (SNOE) or absence (SNO) of an applied electric field. Density functional theory (DFT) calculations including hydrostatic pressure indicate that SNO's ferroelectricity remains up to 25 GPa in the structure of space group  $Cmc2_1$  derived from the condensation of one zone-center soft phonon. The predicted DFT theoretical structural changes are discussed and compared with the results of the experimental Raman spectra as a function of pressure. The pressure-dependent spectra were recorded from atmospheric pressure up to 11.5 and 13.5 GPa for SNOE and SNO, respectively. Both samples underwent a pressure induced phase transition from an incommensurate to a commensurate state at room temperature, SNO at  $P_{i-c} = 6.5 \pm 0.2$  GPa, and SNOE at  $P_{i-c} = 6.9 \pm 0.3$  GPa. The DFT calculations enable the identification of the change in phase to the orthorhombic structure with the space group  $Cmc2_1$ . The experimental values for  $P_{i-c}$  are in reasonably good agreement with the theoretical predicted value of  $\sim 7.3$  GPa. After the critical pressures, the number of observable phonons decreases, that is, when the compound adopts a higher symmetry structure, several phonons vanish abruptly in both the SNO and SNOE samples, as expected. The Raman spectra for both samples show hysteresis effects, that is, after the pressure is removed, a few extra lines remain visible, as well as many relative intensity changes and broadenings for some phonon bands. The bulk moduli of the  $\text{Sr}_2\text{Nb}_2\text{O}_7$  before and after  $P_{i-c}$  are calculated resulting in 117.0 and 147.8 GPa, respectively. The Grüneisen parameters of the phonons observed are finally calculated and discussed.

DOI: [10.1103/PhysRevB.100.054110](https://doi.org/10.1103/PhysRevB.100.054110)

**I. INTRODUCTION**

Perovskites and perovskite-layered compounds are very interesting and attractive families of materials that exhibit a wide variety of interesting physical properties, such as piezoelectricity, ferroelectricity, magnetism, superconductivity, and multiferroic behaviors. Their properties have found many applications such as photovoltaic active compounds in solar cells [1], in perovskite electroluminescent diodes and optically pumped lasers [2], and in next-generation photodetectors [3].

For many perovskites, several of the aforementioned properties may coexist in a given compound, as they are successively revealed at different temperatures or applied pressure ranges, where the compound adopts different structural phases, which in turn provide the physical conditions that allow the manifestation of a given property.

For instance,  $\text{PbTiO}_3$  perovskite, which adopts a tetragonal phase below 13 GPa, followed by a “transition region” where

the crystal adopts a “close to” cubic phase, to finally adopt another tetragonal form at 18 GPa [4], or  $\text{BaTiO}_3$ , which in an analogous way has a ferroelectric tetragonal structure at zero pressure up to 2.7 GPa, where it adopts a cubic paraelectric phase, to revert to some ferroelectric undetermined lower symmetry phase above 5 GPa [5].

Of particular interest is the phase transitions in simple perovskite compounds  $ABX_3$  under hydrostatic pressure, which is a very active investigation area with great relevance to application-related issues. From these investigations, some general rules were formulated for the behavior of phase transitions in perovskite-type compounds under hydrostatic pressure: (a) there is a decrease in the transition temperature for perovskites that present soft zone-center distortion and octahedral rotations with small compressibility factors for the  $A-X$  bond [6–8] and (b) there is an increase in the phase transition temperature for perovskites that present octahedral rotations with rigid  $BX_6$  octahedra [6–8].

For laminar perovskites with the general formula  $A_nB_nX_{3n+2}$  ( $n$  is the number of  $BX_6$  octahedra per layer; octahedral distortion and tilting lower the symmetry of these phases, hereafter called Brandon-Megaw compounds [9]),

\*Corresponding authors: carmen.aranda@uaslp.mx; hnavarro@uaslp.mx

**EL ESTADO DE BIENESTAR COMO  
UN BIEN PÚBLICO NO EXCLUIBLE**

**THE WELFARE STATE AS A  
PUBLIC GOOD NOT EXCLUDABLE**

**Elvio Accinelli**

*Universidad Autónoma de San Luis Potosí*

**Oswaldo Salas**

*Universidad de Gotemburgo*

*Resumen:* Se analiza la posible evolución de una economía en la que, hasta cierto momento, el Estado actuaba como monopolista en la prestación de un conjunto de servicios públicos y que, ante un cambio en la situación económica, se plantea la interrogante acerca de que si estos servicios deben seguirse prestando por parte del Estado o bien deben pasar a manos de particulares. Con independencia de la respuesta a tal cuestionamiento, se supone que dichos servicios deben prestarse sin exclusiones y con la misma calidad a todos los ciudadanos al margen de su riqueza. Este es un principio básico que pauta las economías de los países que, como Suecia, se rigen por las normas del estado de bienestar.

*Abstract:* In this work, we analyze the possible evolution of an economy in which, up to a certain point, the State acted as a monopolist in the provision of a set of public services and, faced with a change in the economic situation, poses itself, the question about whether these services should continue to be, as they were until then, provided by the State or, if the service should be handed over to private individuals. Regardless of the answer to this question, it is assumed that they should be provided without exclusions and with the same quality to all citizens regardless of their wealth. This is a basic principle that guides the economies of countries that, like Sweden, are governed by the rules of the welfare state. We introduce a model based on game theory to analyze the evolution of this process and its possible outcomes.

*Clasificación JEL/JEL Classification: H30, H44, B05*

*Palabras clave/keywords: estado de bienestar; teoría de juegos; privatización; welfare state; game theory; privatization*

*Fecha de recepción: 21 VIII 2017*

*Fecha de aceptación: 02 IV 2018*

*Estudios Económicos, vol. 34, núm. 2, julio-diciembre 2019, páginas 243-273*

## Improvement in the dispersion of TiO<sub>2</sub> particles inside Chitosan-Methyl cellulose films by the use of silane coupling agent

---

Enrique Delgado Alvarado<sup>1</sup>, Mariana Gisela Peña Juárez<sup>1</sup>, Cristina Pérez Pérez<sup>2</sup>, Elias Pérez<sup>3</sup>, José Amir González Calderón<sup>4\*</sup>.

<sup>1</sup>Doctorado Institucional en Ingeniería y Ciencias de Materiales, Universidad Autónoma de San Luis Potosí, Av. Sierra Leona #550, Colonia Lomas 2a. Sección, Lomas de San Luis, 78210 San Luis Potosí, S.L.P., Mexico.

<sup>2</sup> Departamento de Ingeniería Bioquímica, Instituto Tecnológico de Celaya, Garcia Cubas s/n, C.P. 38010, Celaya, Guanajuato. México

<sup>3</sup> Instituto de Física, Universidad Autónoma de San Luis Potosí, Zona Universitaria. Av. Dr. Manuel Nava 6, Lomas, C.P. 78290, San Luis Potosí, SLP, México.

<sup>4</sup> CONACYT - Instituto de Física, Universidad Autónoma de San Luis Potosí, Zona Universitaria. Av. Dr. Manuel Nava 6, Lomas, C.P. 78290, San Luis Potosí, SLP, México.

\*Corresponding author: José Amir González Calderón, e-mail: [amir.gonzalez@oppi.tech](mailto:amir.gonzalez@oppi.tech), [amir@ifisica.uaslp.mx](mailto:amir@ifisica.uaslp.mx)

Received November 22<sup>th</sup>, 2018; Accepted May 24<sup>th</sup>, 2019

DOI: <http://dx.doi.org/10.29356/jmcs.v63i2.741>

**Abstract.** This work is focused on obtaining composite films based on biopolymer of chitosan and on TiO<sub>2</sub> superficially modified through a silanization method, using (3-aminopropyl)-trimethoxysilane (APTMS). This method helped solve specific problems of titanium dioxide, such as the formation of agglomerates, since modified films have a better dispersion. The inclusion of particles in the biopolymer films helped to improve color properties, obtaining luminescence results up to 20% higher than the unmodified particles, which indicates a better dispersion of particles. In addition, there were improvements in the electrostatic repulsion, studied as Z potential, with values of 10 mV for TiO<sub>2</sub> and 27 mV for S-TiO<sub>2</sub>. Finally, better results were obtained in the mechanical properties of the silanized particles, with an improvement of around 28% in low percentages, rising the percentage by increasing S-TiO<sub>2</sub>.

**Keywords:** Silanization; Chitosan; Biopolymers; Films; Materials.

**Resumen.** Este trabajo está enfocado en obtener películas compuestas basadas en el biopolímero quitosán y en TiO<sub>2</sub> modificado superficialmente mediante un método de silanización, utilizando (3-aminopropil) trimetoxisilano (APTMS). Este método ayudó a resolver problemas particulares del dióxido de titanio, como lo son la formación de aglomerados, ya que las películas modificadas tienen una mejor dispersión. La inclusión de partículas en las películas de biopolímeros ayudó a mejorar las propiedades de color, obteniendo resultados de luminiscencia hasta en un 20% mayor que las partículas no modificadas, lo cual es indicador de una mejor dispersión de partículas. También se tuvieron mejoras en la repulsión electrostática, estudiada como potencial Z, con valores desde 10 mV para TiO<sub>2</sub> a 27 mV para S-TiO<sub>2</sub>. Finalmente, también se tuvieron mejores resultados en las propiedades mecánicas de las partículas silanizadas, con una mejora de alrededor del 28% a bajos porcentajes, incrementando valores al aumentar el porcentaje de S-TiO<sub>2</sub>.

**Palabras clave:** Silanización; Quitosán; Biopolímeros; Películas; Materiales.

---

## MEAN SENSITIVE, MEAN EQUICONTINUOUS AND ALMOST PERIODIC FUNCTIONS FOR DYNAMICAL SYSTEMS

FELIPE GARCÍA-RAMOS\*

CONACyT / Instituto de Física, Universidad Autónoma de San Luis Potosí (UASLP)  
Av. Manuel Nava #6, Zona Universitaria, San Luis Potosí, S.L.P., 78290, México

BRIAN MARCUS

Department of Mathematics, University of British Columbia  
Vancouver, BC, V6T 1Z2, Canada

(Communicated by Jairo Bochi)

**ABSTRACT.** We show that a continuous abelian action (in particular  $\mathbb{R}^d$ ) on a compact metric space equipped with an invariant ergodic measure has discrete spectrum if and only if it is  $\mu$ -mean equicontinuous (proven for  $\mathbb{Z}^d$  in [14]). In order to do this we introduce mean equicontinuity and mean sensitivity with respect to a function. We study this notion in the topological and measure theoretic setting. In the measure theoretic case we characterize almost periodic functions with these concepts and in the topological case we show that weakly almost periodic functions are mean equicontinuous (the converse does not hold). We compare our results with some results in the theory of Delone dynamical systems and quasicrystals.

A  $\mathbb{Z}$ -topological dynamical system ( $\mathbb{Z}$ -TDS) is a pair  $(X, T)$  where  $X$  is a compact metric space (with metric  $d$ ) and  $T : X \rightarrow X$  a continuous invertible function (we will deal with abelian  $\mathbb{G}$  actions, but for the introduction using  $\mathbb{Z}$  will be enough to get intuition on the definitions). In the theory of topological dynamical systems several notions of order have been studied. The most ordered systems are the periodic systems, i.e. when for every  $x \in X$  there exists  $n_x > 0$  such that  $T^{n_x}x = x$ ; followed by the equicontinuous systems i.e. when for every  $\varepsilon > 0$  there exists  $\delta > 0$  such that if  $d(x, y) \leq \delta$  then  $d(T^i x, T^i y) \leq \varepsilon$  for every  $i \geq 0$ . This notion means that the system is highly predictable in the following sense: if you only know  $x$  is inside a small  $\delta$ -neighbourhood you will be able to predict with  $\varepsilon$ -precision the orbit of  $x$ . Several weaker notions like distality, nullness, tameness, mean equicontinuity, among others have been studied. In particular we are interested in mean equicontinuity. A system is mean equicontinuous, if for every  $\varepsilon > 0$  there exists  $\delta > 0$  such that if  $d(x, y) \leq \delta$  then  $\limsup \frac{1}{n} \sum_{i=1}^n d(T^i x, T^i y) \leq \varepsilon$ . Here we have predictability not for every  $i$  but on sets of high density (see Proposition 1.23). According to Asulander [2], Fomin introduced these systems in [11].

Mean equicontinuity has received interest in recent years due to connections with ergodic properties of measurable dynamical systems, i.e. dynamical systems

---

2010 *Mathematics Subject Classification.* 37A05, 37A25, 37A35, 37B05.

*Key words and phrases.* Mean equicontinuity, discrete spectrum, quasicrystals, almost periodic functions, mean sensitivity.

\* Corresponding author.



# An algorithm for the *in situ* analysis of optical reflectance anisotropy spectra

J. Ortega-Gallegos<sup>a,\*</sup>, A. Lastras-Martínez<sup>a,\*</sup>, L.E. Guevara-Macías<sup>a</sup>, J.G. Santiago García<sup>a</sup>,  
D. Ariza-Flores<sup>a,b</sup>, R. Castro-García<sup>a,b</sup>, R.E. López-Estopier<sup>a,b</sup>, R.E. Balderas-Navarro<sup>a</sup>,  
L.F. Lastras-Martínez<sup>a</sup>



<sup>a</sup> Instituto de Investigación en Comunicación Óptica, Universidad Autónoma de San Luis Potosí, Alvaro Obregón 64, San Luis Potosí, SLP 78000, Mexico

<sup>b</sup> CONACyT - Instituto de Investigación en Comunicación Óptica, Universidad Autónoma de San Luis Potosí, Alvaro Obregón 64, San Luis Potosí, SLP 78000, Mexico

## ARTICLE INFO

Communicated by R.M. Biefeld

### Keywords:

A1. Characterization  
A1. Growth models  
A1. Surface processes  
A3. Molecular beam epitaxy  
B2. Semiconducting gallium arsenide  
B2. Semiconducting III-V materials

## ABSTRACT

We report on a computer algorithm for the *in situ* analysis of reflectance anisotropy (RA) spectra in a time frame compatible with the epitaxial growth of cubic semiconductors. This algorithm allows for the *in situ* acquisition of RA spectra and their decomposition into two components whose amplitude depends on the As coverage of the semiconductor surface. One of such components is associated with the surface orthorhombic strain due to the surface reconstruction and has an amplitude that strongly depends with surface reconstruction and thus As coverage. This fact opens the possibility of using reflectance anisotropy spectroscopy (RAS) as an optical probe to characterize the As surface coverage in real time. To demonstrate the performance of the algorithm we report on RA measurements carried out during the homoepitaxial growth of GaAs (001). We show that the algorithm is capable of analyzing a set of 500 RA spectra in a time span of about 10 s. This allows for a range of applications for the developed algorithm, including the surface characterization and fine tuning of the substrate stoichiometry just before epitaxial growth, during the growth of the buffer layer.

## 1. Introduction

The growing complexity of advanced optoelectronic devices based on III-V semiconductors [1–3] demands probes for real-time growth monitoring with sub monolayer resolution. Non-invasive optical probes, such as reflectance anisotropy spectroscopy (RAS), are advantageous for this application given their high sensitivity, instrumental simplicity and fast response [4–6]. RAS is an optical polarization contrast technique, based on the measurements of difference of reflectivity for two orthogonal polarized light beams [8]. This spectroscopy enhances the surface related response by taking advantage of the reduced symmetry of the surface region of a cubic crystal. We note that for polarizations of the incident beam parallel to the principal axes of the crystal, the signal arising from the isotropic bulk is suppressed [4,5,9,10].

The usefulness of RAS as a surface characterization technique stems from the strong dependence of the reflectance anisotropy (RA) line shape on surface reconstruction [4–7]. In this respect, GaAs surfaces with reconstructions  $c(4 \times 4)$  and  $(2 \times 4)$  show characteristic and well differentiated RA lineshapes. However, despite the fact that the surface specificity of anisotropic reflectance has been recognized for a long time [11], the development of the full potential of the technique for the

real-time characterization of epitaxial growth has been traditionally hampered by the lack of anisotropic reflectance spectrometers with high enough, both, spectrum acquisition speed and spectral resolution.

Recently, we developed a rapid RA 32-channel spectrometer with the capability to measure in real-time fractional changes of monolayer coverage during epitaxial growth [12]. Taking advantage of such instrument, we carried out a series of real-time RAS measurements during the homoepitaxial growth of GaAs (001) under several  $As_4$  overpressures and found that upon starting growth on an As-rich surface ( $c(4 \times 4)$  reconstruction), the RAS amplitude undergoes a fast transient towards a less As-rich surface ( $(2 \times 4)$  reconstruction). This transient is a function of both As overpressure and substrate temperature and takes place within the first monolayer (ML) growth period.

RA line shapes are, nevertheless, complex and not readily interpreted. Indeed, previously we have shown that the reflectance anisotropy (RA) spectra of both  $c(4 \times 4)$  and  $(2 \times 4)$  surfaces comprise two spectral components whose relative amplitude is a function of surface As coverage [13]. A first component is associated with the orthorhombic strain induced by surface reconstruction and its amplitude changes sign when shifting from  $c(4 \times 4)$  to  $(2 \times 4)$  reconstruction [13]. A second component shows an amplitude variation with no change of sign [16]. Additionally, it is noted that the RAS oscillations are mainly

\* Corresponding authors.

E-mail addresses: [jortega@cactus.iico.uaslp.mx](mailto:jortega@cactus.iico.uaslp.mx) (J. Ortega-Gallegos), [alm@cactus.iico.uaslp.mx](mailto:alm@cactus.iico.uaslp.mx) (A. Lastras-Martínez).

<https://doi.org/10.1016/j.jcrysgro.2019.03.002>

Received 15 November 2018; Received in revised form 5 February 2019; Accepted 1 March 2019

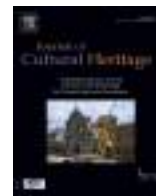
Available online 02 March 2019

0022-0248/ © 2019 Elsevier B.V. All rights reserved.



Available online at  
**ScienceDirect**  
[www.sciencedirect.com](http://www.sciencedirect.com)

Elsevier Masson France  
**EM|consulte**  
[www.em-consulte.com/en](http://www.em-consulte.com/en)



Original article

## Determination of the layered structure of baryta based heritage photographs by infrared ellipsometry



J.M. Flores-Camacho<sup>a,\*</sup>, A. Nieto-Villena<sup>c,b</sup>, J.R. Martínez<sup>d</sup>, J.A. de la Cruz-Mendoza<sup>e</sup>,  
 G. Ortega-Zarzosa<sup>d</sup>, Á. Solbes-García<sup>c</sup>, R.E. Balderas-Navarro<sup>a</sup>, A. Lastras-Martnez<sup>a</sup>

<sup>a</sup> Instituto de Investigación en Comunicación Óptica, Universidad Autónoma de San Luis Potosí, Av. Karakorum 1470, 78210 San Luis Potosí, S.L.P., Mexico

<sup>b</sup> Departamento de Conservación y Restauración de Bienes Culturales, Universitat Politècnica de València, Camino de Vera s/n, 46022 Valencia, Spain

<sup>c</sup> Facultad del Hábitat, Universidad Autónoma de San Luis Potosí, Álvaro Obregón 64, 78000 San Luis Potosí, S.L.P., Mexico

<sup>d</sup> Facultad de Ciencias, Universidad Autónoma de San Luis Potosí, Álvaro Obregón 64, 78000 San Luis Potosí, S.L.P., Mexico

<sup>e</sup> Instituto de Física, Universidad Autónoma de San Luis Potosí, Álvaro Obregón 64, 78000 San Luis Potosí, S.L.P., Mexico

### ARTICLE INFO

#### Article history:

Received 15 February 2018

Accepted 13 September 2018

Available online 15 October 2018

#### Keywords:

Photographic Prints  
 Infrared ellipsometry  
 Gelatin  
 Baryta  
 Julian Carrillo

### ABSTRACT

Variable angle-infrared spectroscopic ellipsometry is proposed as a reliable tool for the characterization of heritage photographic prints. It is shown that the proposed technique has access to both the chemical composition and the physical structure of the photograph. In particular, the physical structure can be determined by interference related spectral oscillations and the behavior, for different angles of incidence, of the peaks corresponding to different chemical components. Emphasis is made on gelatin/baryta samples, and particularly, in the role of the baryta layer. A relatively simple model is used to simulate the ellipsometric spectra. It shows that the thickness and location of different layers in photographic prints can be assessed by optical means.

© 2018 Elsevier Masson SAS. All rights reserved.

### 1. Research aim

The aim of the present work is to present variable-angle infrared-ellipsometry (IRSE) as a reliable tool for the characterization of heritage photographic prints that complements the information obtained from traditional techniques such as Fourier-transform infrared spectroscopy and Raman. IRSE has access to amplitude and phase of light signals, when combined with incidence of probing light at different angles, permits the determination of the chemical composition and the multilayered structure of the print.

### 2. Introduction

The artistic and documental value of photographic prints, in particular those from the turn of the 20th century, makes it necessary to take actions for their preservation, which requires an in-depth knowledge of the chemical composition and physical structure of these objects [1]. Access to this information has been

successfully provided by analytical techniques such as electron microscopies, atomic force microscopy, Raman spectroscopy, and Fourier-Transform Infrared spectroscopy (FTIR), among others [1]. Of special interest are those of non-invasive and non-destructive character such as the spectroscopic optical techniques. In particular, FTIR has been used for the identification of pigments and organic components in the photographic colloid [2–4], for identification of organic varnishes [5] possibly used as protective coatings, for the detection of the presence of the baryta layer and, combined with other analyses, identification of sources of biological deterioration [6]. The recently explored terahertz spectral region can be used for the characterization of the paper substrate [7].


Gelatin and colloidion aristotypes were the first kind of photographic papers in which the paper support was submitted to a treatment based on the application of a layer of barium sulfate [8]. This technique was later passed on to the more contemporary silver bromide emulsions based *developing out papers*. The baryta paper [9] provided a better finishing of the print [8] and a separation of the emulsion layer from contaminants of the paper support [6]. The barium sulfate pigment was commonly suspended in gelatin; however, it has been known that gum arabic and albumen were also part of this layer. Wax, casein, milk, and starch, among others, were later introduced in the formulation [8]. The baryta layer was composed mostly of BaSO<sub>4</sub>, but SrSO<sub>4</sub> and titanium dioxide were also part of

\* Corresponding author.

E-mail addresses: [jmflores@cactus.iico.uaslp.mx](mailto:jmflores@cactus.iico.uaslp.mx) (J.M. Flores-Camacho), [alejandra.nieto@uaslp.mx](mailto:alejandra.nieto@uaslp.mx) (A. Nieto-Villena).

## ORIGINAL ARTICLE

# Determination of sialic acid levels by using surface-enhanced Raman spectroscopy in periodontitis and gingivitis

Alondra Hernández-Cedillo<sup>1</sup> | Ma. Guadalupe García-Valdivieso<sup>1</sup> | Aida Catalina Hernández-Arteaga<sup>1</sup> | Nuria Patiño-Marín<sup>2</sup> | Ángel Antonio Vértiz-Hernández<sup>3</sup> | Miguel José-Yacamán<sup>1,4</sup> | Hugo Ricardo Navarro-Contreras<sup>1</sup> 

<sup>1</sup>Coordinación para la Innovación y Aplicación de la Ciencia y la Tecnología (CIACYT), Universidad Autónoma de San Luis Potosí, San Luis Potosí, México

<sup>2</sup>Facultad de Estomatología, Universidad Autónoma de San Luis Potosí, San Luis Potosí, México

<sup>3</sup>Coordinación Académica Región Altiplano de la Universidad Autónoma de San Luis Potosí, Matehuala, S.L.P., México

<sup>4</sup>Department of Physics and Astronomy, University of Texas at San Antonio, San Antonio, Texas, USA

## Correspondence

Hugo Ricardo Navarro-Contreras, Coordinación para la Innovación y Aplicación de la Ciencia y la Tecnología (CIACYT), Universidad Autónoma de San Luis Potosí, Álvaro Obregón 64, San Luis Potosí, S.L.P. 78000, México.  
Email: hnavarro@uaslp.mx

## Funding information

FAI-UASLP; Consejo Nacional de Ciencia y Tecnología, Grant/Award Number: 446208 and 2015-01-986; Welch Foundation, Grant/Award Number: #AX-1615; Laboratorio Nacional de Análisis Físicos, Químicos y Biológicos-UASLP; Clínica de Periodoncia, Facultad de Estomatología, UASLP

## Abstract

**Objectives:** To compare the sialic acid (SA) levels in saliva among periodontitis-affected, gingivitis and control patients.

**Methods:** The study involved 93 subjects. The participants were divided into three groups: (1) 30 subjects without periodontal disease (control group); (2) 30 subjects with gingivitis; and (3) 33 subjects with periodontitis. The oral parameters examined were as follows: (a) Simplified Oral Hygiene Index; (b) Calculus Index; (c) Gingival Index; (d) probing pocket depth; and (e) level of epithelial attachment. SA levels in saliva were measured by means of surface-enhanced Raman spectroscopy (SERS). This method has demonstrated the capacity to detect extremely low concentrations of molecules. The spectrum was calibrated using analytical reagent SA.

**Results:** The obtained median values for SA concentrations were 5.98, 7.32, and 17.12 mg/dl for control, gingivitis, and periodontitis patients, respectively.

**Conclusions:** Our measurements by SERS corroborate that in periodontitis-affected patients, the SA concentration is larger than their concentrations in either control or gingivitis patients. This confirms previous reports and opens the possibility of using SERS as a diagnostic tool.

## KEYWORDS

Ag nanoparticles, gingivitis, periodontitis, sialic acid, surface-enhanced Raman

## 1 | INTRODUCTION

Molecules in saliva have been proposed as useful biomarkers in the diagnostics of several human diseases (Liu & Duan, 2012; Pfaffe, Cooper-White, Beyerlein, Kostner, & Punyadeera, 2011). The simplicity of its recollection and non-person invasiveness are advantages as a diagnostic instrument in certain conditions affecting humans.

Sialic acid (SA) is an important salivary biomarker that is correlated with systemic inflammation (Schauer, Kelm, Reuter, Roggentin, & Shaw, 1995). SA has the chemical formula  $C_{11}H_{19}NO_9$ . SA is part of the glycolipids and glycoproteins that traverse the cellular membrane. A relevant function of this SA attached to the cell membranes is to regulate innate immunity (Liu & Duan, 2012; Pfaffe et al., 2011; Schauer et al., 1995). The dominant form of SA in human fluids, including saliva, is N-acetylneuraminic acid (Varki, Kannagi, & Toole, 2009).

## LOCAL COMPLETENESS, PARETO EFFICIENCY AND MACKEY BISHOP-PHELPS CONES

ELVIO ACCINELLI AND ARMANDO GARCÍA\*

Facultad de Economía UASLP  
Av. Pintores S7N  
San Luis Potosí, CP 78280, México

(Communicated by Onésimo Hernández-Lerma)

**ABSTRACT.** Avoiding usual completeness hypothesis and working on the frame of locally complete spaces some Pareto optimization results are obtained. The Mackey Bishop-Phelps cones are defined and a characterization for the existence of Pareto efficiency respect to these cones is obtained.

**1. Introduction.** In [14], Kuhn and Tucker considered “proper solutions” for vector maximum problems and introduced the concept of proper efficient points. Hurwicz [6] introduced the notion of a proper maximal point with respect to ordering cones to characterize maximal points as solutions for optimization problems. Isac [7, 8, 9, 10, 11] and Fang [5] considered the general optimization problem in topological vector spaces ordered by a closed pointed convex cone. They have several general results on the existence of solutions using the completeness properties of the space or of the related subsets. The method used is based on a general existence theorem for critical points of dynamical systems in complete locally convex spaces. Qiu [22, 23], Bosch, García et al. [3, 4] have found extensions to several variational principles assuming only local completeness conditions for the space or for the related subsets. By adapting ideas of Isac to locally complete spaces some Pareto optimization results are obtained. In particular, in [12] Isac defined the full nuclear cones as a natural extension of the Bishop-Phelps cones to locally convex spaces and obtained a general existence result for Pareto efficiency. Here, by adapting the concept to locally complete spaces, the Mackey Bishop-Phelps cones are defined and a similar result is obtained.

**2. Preliminaries.** Throughout this paper  $(E, \tau)$  will denote a real locally convex space  $E$ , with topology  $\tau$ . A disk  $B$  in  $E$  is a closed, bounded and absolutely convex subset. We denote by  $(E_B, \rho_B)$  the linear span of the disk  $B$  endowed with the topology generated by the Minkowski’s functional associated with  $B$ . Note that  $\rho_B \geq \tau|_{E_B}$ , i.e. the Minkowski’s norm in  $E_B$  is finer than the original topology  $\tau$  restricted to  $E_B$ . So,  $(E_B, \rho_B)$  is continuously embedded in  $(E, \tau)$ . If  $(E_B, \rho_B)$  is a  $\rho_B$ -complete normed space then  $B$  is called a Banach disk.  $(E, \tau)'$  will denote the

---

2010 *Mathematics Subject Classification.* Primary: 49J53; Secondary: 46N10.

*Key words and phrases.* Banach disk, local completeness, generalized dynamical system, nuclear cone, Pareto efficiency.

\* Corresponding author: Armando García.



## FREE MOBILITY OF CAPITAL AND LABOR FORCE IN A TWO-COUNTRY MODEL: THE DYNAMIC GAME FOR GROWTH

ELVIO ACCINELLI\*

Facultad de Economía UASLP  
Av. Pintores S7N  
San Luis Potosí, CP 78280, México

EDGAR SÁNCHEZ CARRERA

DESP University of Urbino Carlo Bo, Italy  
and Associate Researcher at UAdeC, México

LAURA POLICARDO

Ministry of Economy and Finance, Italy

OSVALDO SALAS

School of Public Administration, University of Gothenburg, Sweden

(Communicated by Alejandro Neme)

**ABSTRACT.** In this paper, we consider a two-country and two-sector economy, where firms can choose to be innovative or not innovative, and workers to be skilled or unskilled. Using a dynamic game, we argue that exploiting the comparative advantages a country has in producing goods that use the most abundant factor of production, free mobility of capital and labor is beneficial for economic growth. However, if a country has a comparative advantage in a sector that uses intensely unskilled labor (which is the case of several underdeveloped economies), a poverty trap may arise. For this reason we argue that national Governments must ensure the technological development to improve competitiveness and therefore a social optimal use of the comparative advantages.

**1. Introduction.** Poverty traps are a well-known phenomenon in the economic literature. Several might be the causes: geographic location that prevents human and physical capital accumulation, like for example the lack of access to the sea that prevents the development of commercial relations with other countries, or the prevalence of certain types of diseases affecting health and therefore productivity of workers ([13]). High fertility rates are also a potential cause of poverty traps: fertility indeed tends to be inversely related to women's wages, or the most common

---

2010 *Mathematics Subject Classification.* C70, C73, F12, F16, F20, F42, O30.

*Key words and phrases.* Poverty traps, comparative advantages, imitative behavior, population games.

The authors would like to thank Alejandro Neme as well as an anonymous referee for their useful comments and suggestions to improve this work. Opinions expressed in this publication are those of the authors and do not necessarily reflect the official opinion of the Italian Ministry of Economy and Finance.

\* Corresponding author: Elvio Accinelli.

# Thermoelectric efficiency optimization of nanoantennas for solar energy harvesting

Javier Mendez-Lozoya,<sup>a</sup> Ramón Díaz de León-Zapata,<sup>b</sup> Edgar Guevara,<sup>a,c</sup>  
Gabriel González,<sup>a,c</sup> and Francisco J. González<sup>a,\*</sup>

<sup>a</sup>Universidad Autónoma de San Luis Potosí, LANCYTT—Terahertz National Laboratory,  
San Luis Potosí, S. L. P., México

<sup>b</sup>Tecnológico Nacional de México/I.T. San Luis Potosí, Av. Tecnológico s/n,  
Soledad de Graciano Sánchez, San Luis Potosí S. L. P., México

<sup>c</sup>Universidad Autónoma de San Luis Potosí, Cátedras CONACYT, San Luis Potosí, México

**Abstract.** We compared  $9 \times 9$  arrays of bimetallic Ni(Nickel)-Pt(Platinum) nanoantennas for a classic and evolutive dipole configuration. We fabricated the nanoantennas by e-beam lithography and characterized them with a solar simulator to analyze the  $I - V$  curves. From these curves, a thermoelectric voltage dependence associated by classic and evolutive dipole configuration was observed. We show that the evolutive dipole nanoantennas (EDN) generate up to three times more voltage in contrast with the classic dipole nanoantenna (CDN). Indeed, the evolutive configuration is 1.3 times more efficient than its classical counterpart. The results are corroborated by absorbance of these nanoantennas in the 20 to 36 THz range, where EDN is 40% more efficient than CDN and 30% in the range of 36.1 to 90 THz. Moreover, the experimental results match the thermoelectric behavior obtained using numerical simulations. The EDN can be used in applications ranging from aerospace technology to energy harvesting, photodetector, and sensors, where high thermoelectric efficiency is needed. © 2019 Society of Photo-Optical Instrumentation Engineers (SPIE) [DOI: [10.1117/1.JNP.13.026005](https://doi.org/10.1117/1.JNP.13.026005)]

**Keywords:** thermoelectric effect; classic dipole nanoantennas; evolutive dipole nanoantennas.

Paper 19013 received Jan. 24, 2019; accepted for publication Apr. 9, 2019; published online May 2, 2019.

## 1 Introduction

Harvesting of electromagnetic radiation, capturing visible and infrared radiation using nanodevices has become an essential part to collect renewable energy. For instance, solar cells,<sup>1</sup> solar panels,<sup>2</sup> and photovoltaic cells<sup>3</sup> are common devices based on nanoantennas provided by their ability to efficiently link visible and infrared radiation as well as spatial localized optical fields.<sup>4</sup> To overcome some of the main difficulties for harvesting energy efficiently, we have to compare the use of nanoantennas in applications, such as bolometers and rectennas, where the efficiency decreases with the increase of the thermal-electric effect.<sup>5</sup> Therefore, to solve this problem, researchers are using Seebeck nanoantennas, which are bimetallic nanostructures, with the ability to convert infrared electromagnetic radiation to electric energy.<sup>6</sup> This advantage allows the possibility of using the wasted thermal energy on the range of 2 to 11  $\mu\text{m}$  associated with an increase in temperature from 400 to 2000 K.<sup>7,8</sup> Recently, the electrical efficiency of nanoantennas as a function of their size, shape, and materials at THz frequencies has been studied applying an evolutionary algorithm, where it was shown that, with the use of Bézier curves, it was possible to obtain a geometry that maximizes the thermoelectric efficiency of this device.<sup>9,10</sup> More recently, a numerical method that guaranteed maximum efficiency applying evolutionary algorithms was applied in Ref. 11, where it was demonstrated that, with the use of Bézier curves, it was possible to obtain an optimal geometry for a dipole nanoantenna.

In this work, several devices were fabricated based on bimetallic nanoantennas, consisting of nanostructured elements, with symmetric geometry. The nanoantennas consist of  $9 \times 9$  elements

---

\*Address all correspondence to Francisco J. González, E-mail: [javier.gonzalez@uaslp.mx](mailto:javier.gonzalez@uaslp.mx)

# Surface-enhanced Raman scattering of hydroquinone assisted by gold nanorods

Rodrigo Cabrera-Alonso,<sup>a</sup> Edgar Guevara,<sup>a,b,\*</sup> Miguel G. Ramírez-Elías,<sup>c</sup> Benjamín Moncada,<sup>d</sup> and Francisco J. González<sup>a</sup>

<sup>a</sup>Universidad Autónoma de San Luis Potosí, Terahertz Science and Technology Center and Science and Technology National Lab, San Luis Potosí, Mexico

<sup>b</sup>CONACYT-Universidad Autónoma de San Luis Potosí, San Luis Potosí, Mexico

<sup>c</sup>Universidad Autónoma de San Luis Potosí, Facultad de Ciencias, San Luis Potosí, Mexico

<sup>d</sup>Hospital Central "Dr. Ignacio Morones Prieto," Universidad Autónoma de San Luis Potosí, Zona Universitaria, Dermatology Department, San Luis Potosí, Mexico

**Abstract.** Melasma is an abnormal acquired skin hyperpigmentation disorder, typically on the face, of unknown origin. It is considered a single disease and very little has been found regarding its pathogenesis. Hydroquinone, an aromatic organic molecule, has been considered as the gold standard substance for dermatological melasma treatment. This substance at high concentrations being absorbed by the skin may produce counterproductive disorders, such as blue or brownish-blue colored skin. In recent years, optical techniques based on the interaction of light with biological samples have become innovative methods for medical applications. We used Raman spectroscopy and surface-enhanced Raman spectroscopy (SERS), to evaluate hydroquinone cation radicals *in vitro* at relatively low concentrations, laying the foundation for future biomedical applications. We present the experimental and simulated Raman signal in the presence of hydroquinone at concentrations as low as 0.1 M, as well as the experimental SERS signal assisted by gold nanorods obtained for the same molecule, which presents an electromagnetic enhancement factor of  $\sim 10^4$ . © 2019 Society of Photo-Optical Instrumentation Engineers (SPIE) [DOI: [10.1117/1.JNP.13.036006](https://doi.org/10.1117/1.JNP.13.036006)]

**Keywords:** melasma; hydroquinone; Raman spectroscopy; spectroscopy and surface-enhanced Raman spectroscopy.

Paper 19024 received Feb. 15, 2019; accepted for publication Jun. 25, 2019; published online Jul. 17, 2019.


## 1 Introduction

Raman spectroscopy is an optical technique based on the interaction of light with matter, resulting in valuable information related to the properties of materials. It has been an outstanding technological advancement with many applications in areas such as physics, chemistry, medicine, and biology, among others.<sup>1-3</sup> As a nondestructive technique for biological samples, it provides a unique fingerprint for the molecular structure, which has been analyzed to determine the vibrational, rotational, and low-energy modes of a system. The Raman effect is based on the inelastic scattering of light due to the shift in photon energy when light interacts with matter, where approximately one out of  $10^7$  photons is scattered at different wavelengths due to the gain or loss of energy by inelastic collisions with molecules.<sup>4</sup> The advantages of Raman spectroscopy among other spectroscopic techniques are its relatively low cost and compact instrumentation (portability), its ability to quantify biomolecules in the biological area, and its noninvasiveness for medical applications, with the particular advantage of being employable for a wide range of sample types with minimal processing. For biological samples, this technique has the disadvantages of possible laser photodamage and a low limit of detection. Due to the low signal that occurs in conventional Raman spectroscopy for biological samples, a variety of nanoparticle

---

\*Address all correspondence to Edgar Guevara, E-mail: [eguevara@conacyt.mx](mailto:eguevara@conacyt.mx)

# Performance Improvement of Refractometric Sensors Through Hybrid Plasmonic–Fano Resonances

Mahmoud Hamdy Elshorbagy, Alexander Cuadrado, Gabriel González 

Francisco Javier González , Senior Member, IEEE, Senior Member, OSA, and Javier Alda , Member, OSA

**Abstract**—In this paper, we present a plasmonic refractometric sensor that works under normal incidence; allowing its integration on a fiber tip. The sensor’s material and geometry exploit the large scattering cross section given by high contrast of the index of refraction subwavelength dielectric gratings. Our design generates a hybrid plasmonic–Fano resonance due to the interference between the surface plasmon resonance and the grating response. We optimize the sensor with a merit function that combines the quality parameter of the resonance and the field enhancement at the interaction volume where the plasmon propagates. Our device shows a high sensitivity (1000 nm/RIU) and a high figure of merit (775 RIU<sup>-1</sup>). Degradation in performance is negligible through a wide dynamic range up to 0.7 RIU. These quantitative parameters overperform compared to similar plasmonic sensors.

**Index Terms**—Fano resonances, optical sensors, plasmonics.

## I. INTRODUCTION

**P**HOTONIC nanostructures control light propagation through optical media. They can function as perfect absorbers [1], [2], efficient scatterers [3], [4], frequency selective surfaces [5]–[7], etc. Optical sensors based on surface plasmon resonances (SPR) benefit from the use of nanostructures for an increased range of applications with improved performance. For example, they are applied to colorimetry [8], and refractometers for gases [9], bio-fluids [10], and chemicals [11]. A change in refractive index of the media can be measured with a conventional plasmonic device in Kretschmann configuration, where

Manuscript received January 7, 2019; revised February 28, 2019; accepted March 17, 2019. Date of publication March 27, 2019; date of current version May 23, 2019. This work was supported in part by Ministerio de Economía y Competitividad of Spain (MINECO) under Grant TEC2013-40442 and in part by Ministry of Higher Education of Egypt (MOHE) (missions section). The work of F. J. González was supported in part by Project 278291 (SRECONACYT), in part by Project 105 of “Centro Mexicano de Innovación en Energía Solar,” and in part by the National Laboratory Program from Consejo Nacional de Ciencia y Tecnología de México (CONACYT) through the Terahertz Science and Technology National Lab (LANCYTT). (Corresponding author: Javier Alda.)

M. H. Elshorbagy is with the Applied Optics Complutense Group, Faculty of Optics and Optometry, University Complutense of Madrid, 28037 Madrid, Spain, and also with the Physics Department, Faculty of Science, Minia University, 61519 El-Minya, Egypt (e-mail: mahmouha@ucm.es).

A. Cuadrado and J. Alda are with the Applied Optics Complutense Group, Faculty of Optics and Optometry, University Complutense of Madrid, 28037 Madrid, Spain (e-mail: a.cuadrado@pdi.ucm.es; javier.alda@ucm.es).

G. González and F. J. González are with the Universidad Autónoma de San Luis Potosí, 78210 San Luis Potosí, México (e-mail: gabriel.gonzalez@uaslp.mx; javier.gonzalez@uaslp.mx).

Color versions of one or more of the figures in this paper are available online at <http://ieeexplore.ieee.org>.

Digital Object Identifier 10.1109/JLT.2019.2906933

the reflectance dip is located and measured angularly [12]. In this setup, the key aspects for device performance are: the material and thickness of the metal layer, the refractive index of the prism, the angle of incidence, and the wavelength of the resonance. For angular interrogation, the maximum theoretical value of sensitivity of a Kretschmann configuration based sensor is 600 deg/RIU [12]. This extreme value is achieved with a low index prism ( $n = 1.32$ ) and an angle of incidence of  $\sim 81^\circ$ . The need of a low index of refraction is strongly limited by material availability. Some polymers, such as Cytop, reach very low values of the index of refraction ( $n_{\text{Cytop}} = 1.34$ ) [13]. Here, we select magnesium fluoride,  $\text{MgF}_2$  ( $n_{\text{MgF}_2} = 1.37$ ), because it is commercially available, transparent within the spectral region of interest ( $\lambda \in [1300, 2000]$  nm), and has a very low index of refraction. Moreover,  $\text{MgF}_2$  produces planar interfaces when coating nanostructured reliefs [14]. The angle of incidence and material constrains of Kretschmann configuration lead to a narrow dynamic detection range [12]. To overcome this limit, the community has proposed different configurations of SPR sensors; including spectral interrogation and more sophisticated geometries [15]–[19].

The performance parameters of a SPR sensor are: sensitivity, Figure of Merit (FOM), resolution, linearity, dynamic range, and reproducibility [20]. Sensitivity is the shift of a measurable parameter of the device (a dip in reflectance, transmission, absorption, phase, temperature, etc.) respect to a controlled variable (angle, wavelength, power, etc.) due to a change in the sensed property (refractive index, specimen concentration, color, etc.) [20]. FOM combines sensitivity and the spectral line-shape characteristics in a parameter that compares sensors, independent from the interrogation strategy (angular, spectral, etc.). Resolution is the minimum change of the sensed property measured by the device. Linearity is assured if sensitivity is constant through the entire dynamic range of the sensor. Although high linearity response devices have been reported, the measured shift is not fully linear [16]. The dynamic range is the interval of the sensed property where the sensor works optimally. In refractometric sensors, recent contributions show high efficiency devices with wide dynamic range up to 0.5 RIU [15]–[19], including devices with adjustable dynamic range [21]. In summary, it is very challenging to design an efficient sensor with high sensitivity, large FOM, good resolution, linearity, wide dynamic range, reliability and reproducibility.

Many approaches enhance performance of SPR optical sensors with bi-metals [22], buffer layers [23], and nanoparticles

# Q-switching and mode locking pulse generation from an all-fiber ring laser by intermodal acousto-optic bandpass modulation

E Hernández-Escobar<sup>1</sup>, M Bello-Jiménez<sup>1</sup>, R López-Estopier<sup>1,2</sup>,  
A Camarillo-Avilés<sup>1</sup>, O Pottiez<sup>3</sup>, M A García-Ramírez<sup>4</sup>, M Durán-Sánchez<sup>2,5</sup>,  
B Ibarra-Escamilla<sup>5</sup> and M V Andrés<sup>6</sup>

<sup>1</sup> Instituto de Investigación en Comunicación Óptica (IICO), Universidad Autónoma de San Luis Potosí, Av. Karakorum No. 1470 Lomas 4ª Secc., 78210 San Luis Potosí, Mexico

<sup>2</sup> Consejo Nacional de Ciencia y Tecnología (CONACYT), Av. Insurgentes Sur No. 1582, Col. Crédito Constructor, Del. Benito Juárez, México, D.F. 039040, Mexico

<sup>3</sup> Centro de Investigaciones en Óptica (CIO), Loma del Bosque No. 115, Col. Lomas del Campestre, León, Guanajuato 37150, Mexico

<sup>4</sup> Universidad de Guadalajara, Research Centre for Applied Sciences and Engineering (CUCEI), Electronics and Computer Sciences Dep. Blvd. Marcelino García Barragán No. 1421, Esq. Calzada Olímpica, 44430, Guadalajara, Jalisco, Mexico

<sup>5</sup> Instituto Nacional de Astrofísica, Óptica y Electrónica (INAOE), Luis Enrique Erro No 1, Departamento de Óptica, 72000 Puebla, Mexico

<sup>6</sup> Universidad de Valencia, Departamento de Física Aplicada y Electromagnetismo, ICMUV, c/Dr. Moliner 50, Burjassot, 46100 Valencia, Spain

E-mail: [miguel.bello@uaslp.mx](mailto:miguel.bello@uaslp.mx)

Received 25 August 2018

Accepted for publication 8 October 2018

Published 20 November 2018



CrossMark

## Abstract

Q-switched and mode-locked (QML) pulse generation from an all-fiber ring laser based on intermodal acousto-optic bandpass modulation is reported. The modulator relies on full-acousto-optic mode re-coupling cycle induced by a standing flexural acoustic wave, with a transmission response that is controlled by amplitude modulation of the acoustic wave signal. The Q factor of the cavity is controlled by a rectangular pulse wave with variable frequency and duty cycle, whereas mode locking is achieved by amplitude modulation derived from a standing flexural acoustic wave. The best QML pulses were obtained at 0.5 kHz repetition rate, with a pump power of 549.2 mW, at the optical wavelength of 1568.2 nm. A maximum overall energy of 2.14  $\mu\text{J}$  at an average output power of 1.07 mW was achieved, corresponding to a burst of mode-locked sub-pulses of 100 ps pulse duration within a QML envelope of 3.5  $\mu\text{s}$ .

Keywords: Q-switched and mode-locked, fibre lasers, acousto-optic modulation, fibre optics

(Some figures may appear in colour only in the online journal)

## 1. Introduction

Pulsed fiber lasers have emerged as essential optical light sources for a wide variety of photonic applications [1–5]. For applications involving short or ultrashort pulse generation,

mode locking is the preferred technique, whereas for applications that comprise relatively long and highly energetic optical pulses, Q-switching is the most suitable technique. In this respect, a different type of pulsed regime, called Q-switched mode locking (QML), has been proposed and demonstrated